

Project 115: Final Report

Transmission and Export Cable Fault Detection and Prevention Using Synthetic Aperture Sonar

Prepared for:

New York State Energy Research and Development Authority

Albany, New York

Julian Fraize

Program Manager, National Offshore Wind Research and Development Consortium

Prepared by:

ThayerMahan, Inc.

Groton, Connecticut

Steven Link – Seabed System Group Program Director

Christian Clark – Senior Staff Oceanographer

Welles Sakmar – Engineer

Global Marine Group – OceanIQ

Cherri-Ann Bones – Survey and Route Engineer

State University of New York Maritime College

Paul Kump – Chairperson and Associate Professor

Notice

This report was prepared by ThayerMahan, Inc. (TM), Global Marine Group (GMG), and the State University of New York Maritime College (SUNY) in the course of performing work contracted for and sponsored by the New York State Energy Research and Development Authority (hereafter “NYSERDA”). The opinions expressed in this report do not necessarily reflect those of NYSEDA or the State of New York, and reference to any specific product, service, process, or method does not constitute an implied or expressed recommendation or endorsement of it. Further, NYSEDA, the State of New York, and the contractor make no warranties or representations, expressed or implied, as to the fitness for particular purpose or merchantability of any product, apparatus, or service, or the usefulness, completeness, or accuracy of any processes, methods, or other information contained, described, disclosed, or referred to in this report. NYSEDA, the State of New York, and the contractor make no representation that the use of any product, apparatus, process, method, or other information will not infringe privately owned rights and will assume no liability for any loss, injury, or damage resulting from, or occurring in connection with, the use of information contained, described, disclosed, or referred to in this report.

NYSERDA makes every effort to provide accurate information about copyright owners and related matters in the reports we publish. Contractors are responsible for determining and satisfying copyright or other use restrictions regarding the content of reports that they write, in compliance with NYSEDA’s policies and federal law. If you are the copyright owner and believe a NYSEDA report has not properly attributed your work to you or has used it without permission, please email print@nyserda.ny.gov

Information contained in this document, such as web page addresses, are current at the time of publication.

Preferred Citation

New York State Energy Research and Development Authority (NYSERDA). 2022. “Final Report: Transmission and Export Cable Fault Detection and Prevention Using Synthetic Aperture Sonar,” NYSEDA Report Number 09-22. Prepared by ThayerMahan Groton, CT; Global Marine Group - OceanIQ Chelmsford, England; State University of New York Maritime College New York, New York. nyserda.ny.gov/publications

Table of Contents

Notice	i
Preferred Citation	i
List of Figures	iv
List of Tables	v
Acronyms and Abbreviations	vi
Relevant Software	viii
1 Executive Summary	ES-1
2 Introduction	1
2.1 Methodology.....	1
2.1.1 SeaScout and Equipment	1
2.1.2 Schedule	2
2.1.3 Priority Targets	3
2.1.4 Vessel.....	5
2.2 Survey Metrics.....	6
2.2.5 Current Methodology.....	7
2.2.6 Area Coverage	8
2.2.7 Reporting Requirements	8
2.2.8 Data Processing	8
3 Data Review	10
3.1 Collection and Calibration	10
3.1.1 SAS	11
3.1.2 Multibeam.....	12
3.1.2.1 SeaScout Norbit WBMS.....	13
3.1.2.2 R2Sonic Sonic 2024.....	13
3.1.3 GNSS/USBL.....	14
3.1.4 Laser Scanner.....	15
3.2 Imagery Review.....	16
3.2.1 Existing Cable Routes	16
3.2.2 Existing Infrastructure	16
3.2.3 Environmental Hazards.....	17
3.2.4 Simulated Targets	19

3.3 Mosaics and Surfaces 23

3.4 System Engineering Analysis..... 25

 3.4.1 Hardware Developments..... 26

 3.4.2 Software Developments 26

 3.4.3 Change Analysis 27

 3.4.4 Sensor Comparison 29

3.5 Machine Learning/ATR 30

 3.5.1 Current ATR Details 32

 3.5.2 ATR Considerations 33

 3.5.3 ATR Preliminary Results 34

 3.5.4 ATR Discussion, Analysis 36

 3.5.5 ATR Development..... 39

4 Discussion 41

 4.1 Summary of Current Methodologies 41

 4.2 Limitations of Marine Surveying Technologies 43

 4.3 Key Findings..... 45

 4.4 Relevancy and Market Impact..... 46

 4.5 Future Work..... 48

5 Conclusions..... 50

6 References 52

Appendix A: Calibration and Engineering Analysis 53

Appendix B: Data Package Contents..... 79

Appendix C: ATR Algorithm..... 82

Appendix D: “sGUId” ATR Annotation Tool 87

List of Figures

Figure 1. Survey Areas.....	3
Figure 2. Target Deployment Design.....	4
Figure 3. Simulated Cable Cross Section.....	5
Figure 4. Berto Miller.....	6
Figure 5. Sensor Workflow.....	11
Figure 6. Target D EVT.....	12
Figure 7. USBL and Multibeam Dual Mount.....	14
Figure 8. Vessel Reference Frame.....	15
Figure 9. BIWF SAS Cable Crossings and Mattressing.....	16
Figure 10. BIWF Wind Turbine Foundations.....	17
Figure 11. Hazards Around Infrastructure and Cables.....	19
Figure 12. SAS Continuous Target Image.....	20
Figure 13. Cable Target Intensity Comparison.....	21
Figure 14. Cable Target Imagery Comparison.....	23
Figure 15. BIWF Mosaic.....	24
Figure 16. Simulated Target Post-Recovery SAS Comparison.....	28
Figure 17. Historical SAS Imagery Comparisons.....	29
Figure 18. Bathymetric and SAS Imagery Comparisons.....	30
Figure 19. AI Tagged SAS Imagery.....	32
Figure 20. Comparison of Actual and Predicted Annotations.....	35
Figure 21. ATR False Identification.....	37
Figure 22. Confusion Matrix of ATR Performance.....	39
Figure A- 1. USBL Pole.....	53
Figure A- 2. MRU.....	55
Figure A- 3. Benchmark 9050 C 2014.....	57
Figure A- 4. Temporary Benchmark.....	59
Figure A- 5. GNSS Health Check Positioning.....	61
Figure A- 6. Heading Health Check.....	63
Figure A- 7. GAMS Verification.....	64
Figure A- 8. Vertical Transformation Verification.....	66
Figure A- 9. Sound Speed Comparison.....	68
Figure A- 10. USBL Calibration.....	70
Figure A- 11. MBES Patch Test.....	71
Figure A- 12. Patch Test: Roll.....	70
Figure A- 13. Patch Test: Pitch.....	71
Figure A- 14. Patch Test: Yaw.....	71
Figure A- 15. Sound Speed Profiles.....	75
Figure C- 1. Class Labels.....	86
Figure D- 1. Labelling Annotation Tool.....	87

List of Tables

Table 1. Comparison of Target Intensity.	21
Table 2. Number of Tiles in each of the Dataset Partitions, before and after Augmentation.	36
Table A- 1. DCR Results.....	54
Table A- 2. Equipment.....	56
Table A- 3. Position Control Checks.	58
Table A- 4. TBM Position.....	59
Table A- 5. GNSS Health Check.....	60
Table A- 6. Heading Health Check.....	62
Table A- 7. Vertical Tide Check.	65
Table A- 8. Bar Check.	67
Table C- 1. AI ATR Study Results.....	82
Table C- 2. ATR Precision Scores.....	83
Table C- 3. Class Distribution.....	84
Table C- 4. Ablation Study.....	85

Acronyms and Abbreviations

ACR	Area Coverage Rate
ASV	Autonomous Surface Vehicle
ATR	Automatic Target Recognition
AUV	Autonomous Underwater Vehicle
BIS	Block Island Sound
BIWF	Block Island Wind Farm
BOP	Balance of Plant
cm	Centimeter
DCR	Dimensional Control Report
DIMCON	Dimensional Control
DVL	Doppler Velocity Logger
DP	Dynamic Positioning
EVT	Error Verification Test
FM	Frequency Modulated Pulse
GAMS	GNSS Azimuth Measurement Systems
GB	Gigabytes
GNSS	Global Navigation Satellite System
GPS	Global Positioning System
Hz	Hertz
IMU	Inertial Measurement Unit
INS	Inertial Navigation System
IoU	Intersection-over-union
kHz	Kilohertz
km	Kilometer
km ²	Kilometers Squared
km ² /hr	Kilometers Squared per Hour
kts	Knots
kV	Kilovolt
LIS	Long Island Sound
LTSM	Long Short-term Memory
m	Meter
mAP	Mean Average Position
MBES	Multibeam Echosounder
MINSAS	Miniature Interferometric Synthetic Aperture Sonar
MRU	Motion Reference Unit
mm	Millimeter
MW	Megawatt
NOWRDC	National Offshore Wind Research and Development Consortium
NTRIP	Networked Transport of RTCM via Internet Protocol
NYSERDA	New York State Energy Research and Development Authority
NYSNET	New York State Spatial Reference Network
PAM	Passenger Accommodation Module
RAS	Real Aperture Sonar
ROV	Remotely Operated Vehicle

RP	Reference Point
SAS	Synthetic Aperture Sonar
SBP	Sub-bottom Profiler
SOW	Statement of Work
SSS	Side Scan Sonar
SVP	Sound Velocity Profiler
TB	Terabytes
TBM	Temporary Benchmark
USBL	Ultra-Short Baseline
USD	United States Dollar
UXO	Unexploded Ordnance
VOO	Vessel of Opportunity
YOLO	You Only Look Once

Relevant Software

CARIS HIPS and SIPS

- Manufacturer: Teledyne
- Software Version: 11.4

CARIS Onboard

- Manufacturer: Teledyne
- Software Version: 2.3

Hypack Survey

- Manufacturer: Xylem
- Software Version: 2021

QGIS

- Manufacturer: QGIS (Open Source)
- Software Version: 3.22.2

INSIGHT

- Manufacturer: Kraken Robotics inc.
- Software Version: 0.12.2

SoundSpeedManager

- Manufacturer: HydrOffice
- Software Version: 2022.1.0

1 Executive Summary

Export and transmission cables are critical links in the generation of offshore wind energy and their continued operation is vital for the sustainment of the electrical grid. The offshore wind industry is expanding at a significant rate in the United States, as well as internationally. The Paris Climate Agreement is a substantial driver in this movement as it pursues a global climate objective of reaching net zero emissions by 2050. Offshore wind farms have the potential to be large contributors in reaching this target. In order to maximize the production from offshore wind it is imperative to regularly maintain these cables as to minimize downtime and prevent unplanned outages. This project aimed to isolate potential causes for cable failure and the possible impact of mitigation with preventative maintenance Synthetic Aperture Sonar (SAS) surveys.

In April of 2022, ThayerMahan Inc. deployed aboard the Miller's Launch vessel, Berto Miller, as part of a contract fulfillment under NYSERDA and the National Offshore Wind Research and Development Consortium (NOWRDC). The goal was to deploy the SeaScout system to utilize the technical capabilities of the SAS system to efficiently and accurately (1) identify and map existing cable infrastructure to demonstrate (2) short-term, small-scale changes in bathymetry and (3) create a representative database of SAS imagery to simulate exposed cable sections.

This study used emplaced 33 kV inter-array offshore wind power cables to assess the abilities of the SAS system to detect subsea cables and potential damage. The sections of cable were damaged prior to deployment with increasing severity of failure modality based on results of a previous report. The data analysis incorporated positional analyses, image intensity returns, historical data comparisons, and ThayerMahan's automatic target recognition software. The findings of this report indicate that the SeaScout's synthetic aperture sonar system is capable of identifying cables, assessing damage or movement, and that the automatic target recognition software in its current state is capable of delineating damage versus undamaged cables. Based on the results of this study the SeaScout system accomplished three tasks listed above and would be a complimentary technology with current industry standard survey techniques.

2 Introduction

2.1 Methodology

The test period consisted of onshore mobilization, calibration, and demobilization days as well as an at-sea operational period. During the at-sea operational period, additional equipment integration and calibrations occurred, followed by three distinct survey sub-events that were designed to evaluate the efficacy of the SeaScout system in accomplishing the four cable failure tasks (as listed in Agreement 115). These tasks would set out to determine the application of SAS on for analyzing and determining changes to the environment and infrastructure, as well as comparison to additional sensor data.

- 1) Detect evidence of fishing gear in the vicinity of cables.
- 2) Detect cable movement.
- 3) Detect seabed movement.
- 4) Detect cable damage where exposed.

2.1.1 SeaScout and Equipment

The SeaScout System consists of a towed vehicle (SeaScout) with Synthetic Aperture Sonar (SAS) and either multibeam echosounder and/or laser scanning payloads, a smart-winch, and a communications suite. The core feature of the SeaScout is the AquaPix Miniature Interferometric Synthetic Aperture Sonar (MINSAS). For the SeaScout configuration, three modular arrays are installed along the port and starboard sides of the vehicle that total 180 centimeter (cm) in the along-track length. These dual arrays enable an area coverage rate (ACR) of up to 3 km²/hr and a range independent resolution of 3 cm² out to 200 meters (m). Georeferencing the data is accomplished through a blended solution of data inputs derived from the main vessel's global navigation satellite system (GNSS) inertial navigation system (INS), the vehicle's onboard INS, an ultra-short baseline (USBL) acoustic positioning system, and a Doppler Velocity Logger (DVL). The combined positioning solution results in sub-meter target positioning accuracy capabilities. During operations, the system collects over 300 gigabytes (GB) of data per hour. Data is presented via an operator interface known as SASVIEW, which includes both the real-aperture sonar (RAS) and SAS data. Additionally, the operator can track individual array statuses, environmental conditions, sonar configuration (ping rate, pulse length, etc.), and vessel parameters. The vehicle is also equipped with an integrated Norbit WBMS multi-beam echosounder (MBES) which will simultaneously collect multibeam data during operations.

2.1.2 Schedule

The survey was broken down into three distinct sub-events to satisfy the four survey tasks mentioned previously. Survey sub-event one focused on fixed objects in the test area to characterize system accuracy and repeatability, and allow for adjustments in configuration, equipment, and processing as needed. Results will determine system capabilities and benefits for accomplishing cable failure task 2 (cable movement) and cable failure task 3 (seabed feature movement). Survey sub-event two collected data on simulated cable failures utilizing emplaced targets in the testing site. This enabled a controlled experiment in an environment representative of future wind farm infrastructure. Failure types and severity were assessed as detectable with SAS or detectable by alternate means (e.g., optical payload). This addressed cable failure task 4. Survey sub-event three focused on real-world targets at the Block Island Wind Farm (BIWF). Data was compared against historical surveys with the proposed technology from 2020 (where applicable) to address cable failure tasks 2 and 3. Concurrently, imagery collected during this survey event characterizes the seafloor up to 200-meters on either side of the transmission cable and addressed cable failure task 4 in the event of simulated exposed, damaged cable. Survey events were ordered to prioritize optimal at-sea environmental conditions for testing events.

April 16 – Equipment packed out and inventoried (Groton, CT).

April 17 – Support equipment and SeaScout system loading onto transport trucks (Groton, CT).

April 18 – Mobilization Day 1 (Staten Island, NY)

April 19 – Mobilization Day 2 (Staten Island, NY).

April 20 – Shoreside systems testing, checkout, and calibrations (Staten Island, NY).

April 21 – Departure and transit to calibration site in Long Island Sound (LIS).

April 22 – Calibration and testing (LIS).

April 23 – Block Island survey day 1 (BIWF).

April 24 – Block Island survey day 2 (BIWF).

April 25 – Transit to LIS, target deployment, and initial survey (LIS).

April 26 – Target survey (LIS).

April 27 – Target survey and target recovery (LIS).

April 28 – Demobilization of equipment (Staten Island, NY).

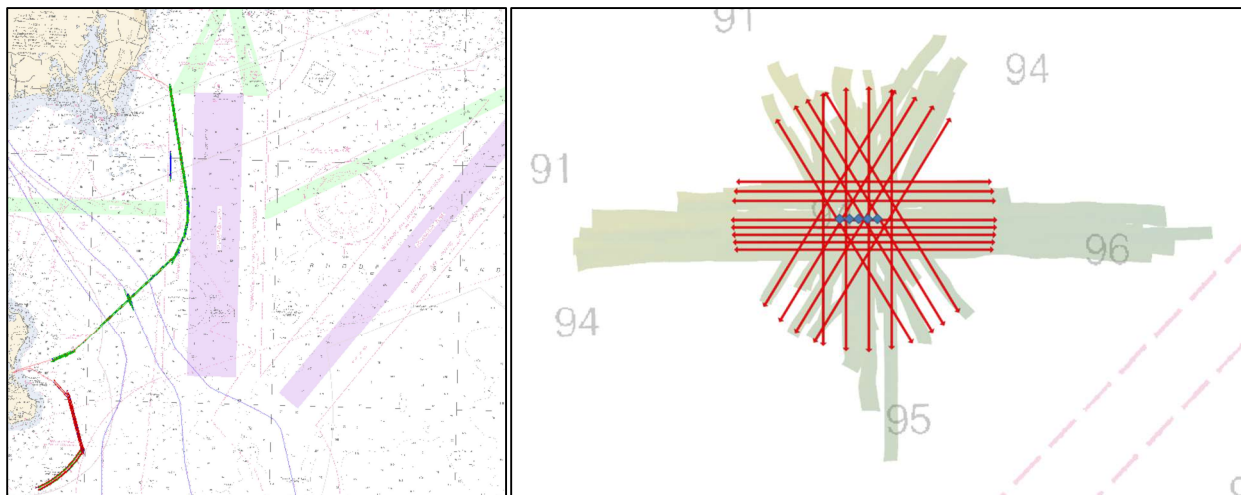
2.1.3 Priority Targets

Survey sub-event three occurred over the BIWF located east of Block Island, Rhode Island in Block Island Sound. The BIWF is the first offshore wind installation on the U.S. East Coast and provided an ideal location due to the existence of historical data, presence of wind farm infrastructure such as foundations and cable mattressing that are anticipated to be similar to future U.S. Northeast offshore wind farms. Survey sub-event two was executed in LIS. The location in LIS was an ideal site for imaging simulated targets. It was chosen due to the paucity of charted seafloor features and protected waters. Locations of both survey event areas can be seen in Figure 1 below.

Figure 1. Survey Areas.

Left chart indicates BIWF survey areas and survey track lines, right chart depicts LIS survey area and target survey track lines (red) with background Norbit MBES.

(ThayerMahan, Inc.)

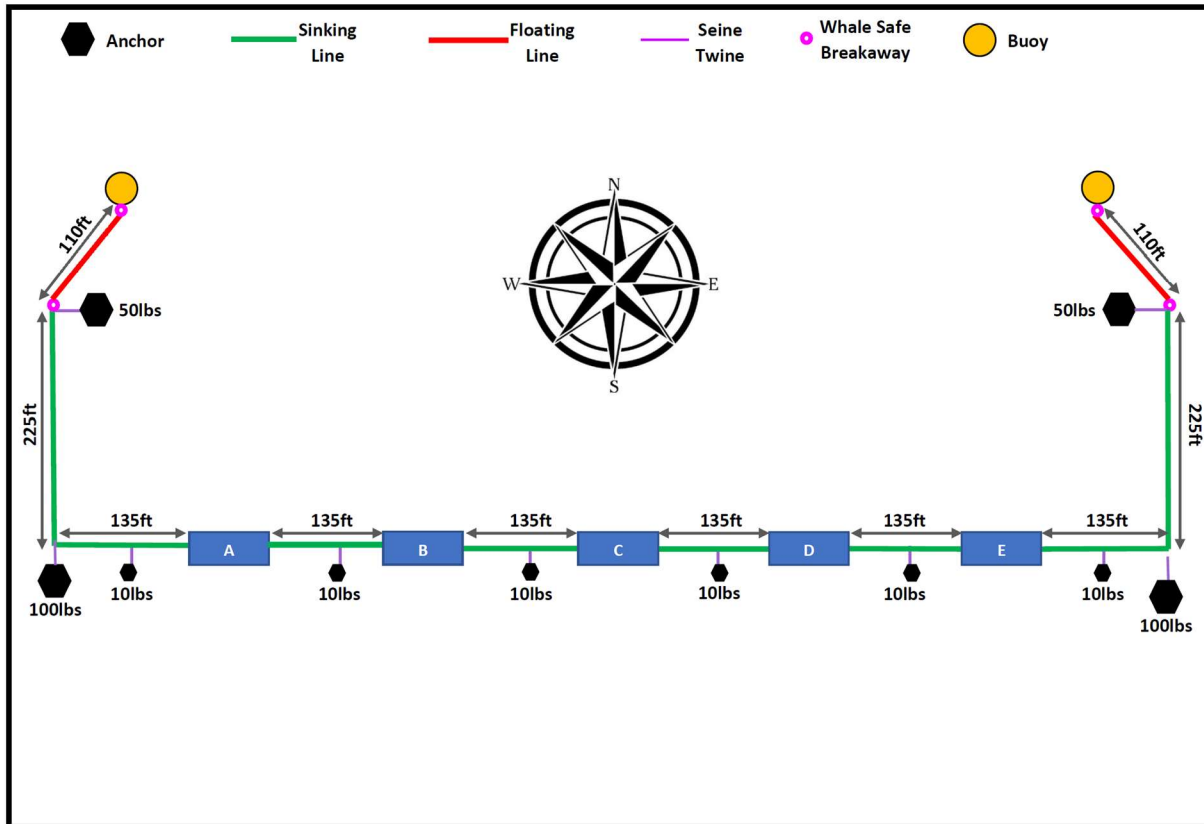


Along with surveying the existing BIWF infrastructure, emplaced targets were deployed to simulate surveying of cables with varying degrees of damage. These targets were deployed in a string such that they could be surveyed at multiple angles and ranges to provide a robust set of imagery for evaluation. The deployed string can be seen in the schematic, Figure 2, below.

Figure 2. Target Deployment Design.

Design schematic of representative cable target deployment in LIS.

(ThayerMahan, Inc.)



The targets themselves consisted of 10-foot sections of 33 kilovolt (kV), 100-millimeter (mm) cable which were strung together at the ends such that the cables would lie long-ways along the seabed once deployed. Each target was damaged at varying degrees of intensity to replicate potential impairment from environmental or physical impacts. These cables replicated standard inter-array cables and their cross-section can be seen in Figure 3 below.

Figure 3. Simulated Cable Cross Section.

Representative cable target.

(ThayerMahan, Inc.)



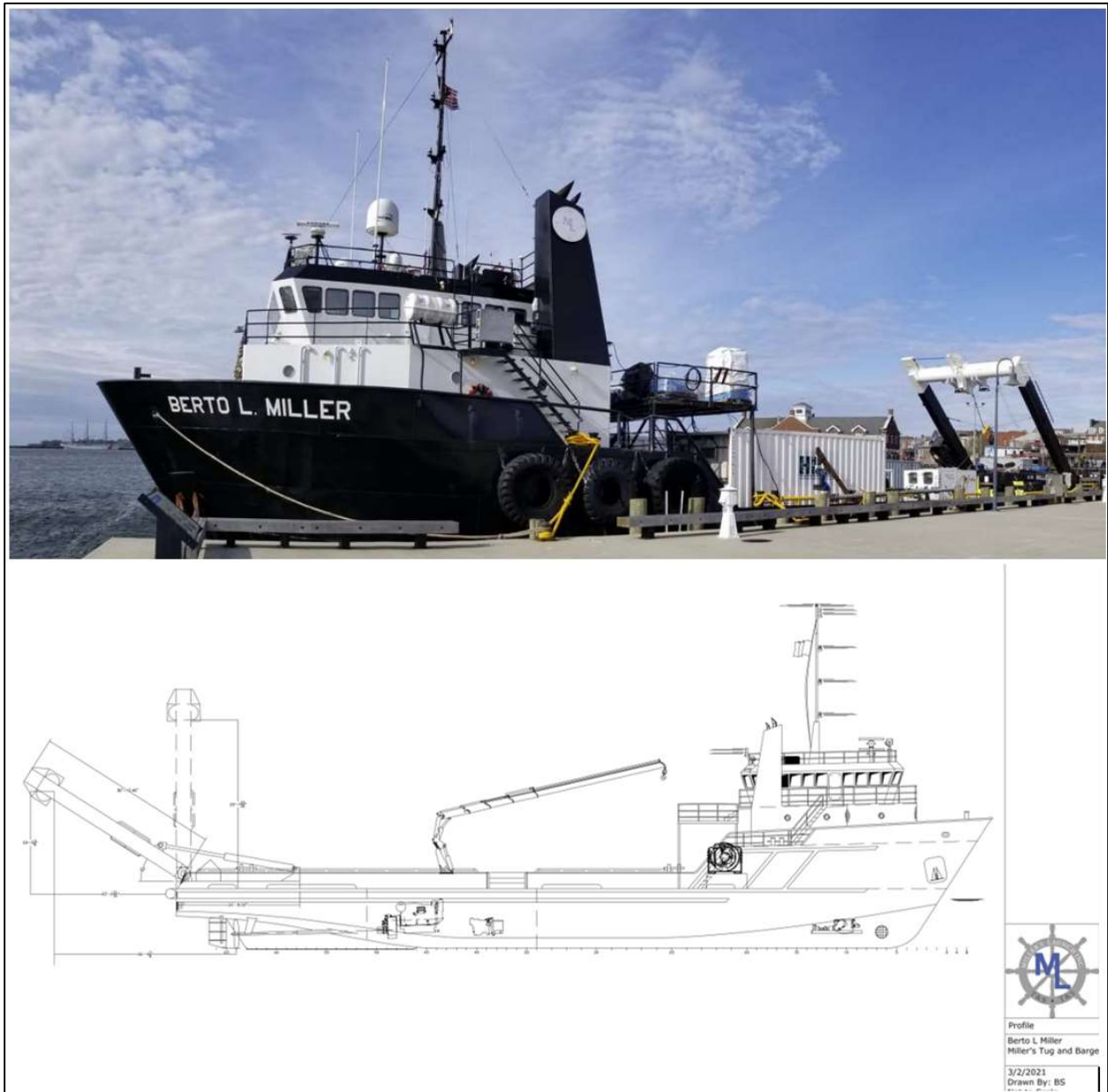
2.1.4 Vessel

The *Berto Miller*, as seen in Figure 4, was utilized as the vessel of opportunity (VOO) for the at-sea survey associated with NYSERDA Contract 115. The *Berto Miller* is a Dynamic Positioning (DP) vessel owned and operated by Miller’s Launch, LLC and provided ideal capabilities for carrying out the survey, deployment, and retrieval tasks successfully and safely. The VOO was mobilized and demobilized in New York Harbor. The SeaScout gear was integrated on-deck and the lab space was setup within a portable Personnel Accommodation Module (PAM).

Figure 4. Berto Miller.

Design schematic (bottom) of *Berto Miller* (top) offshore vessel utilized as vessel of opportunity.

(Miller's Launch, Inc.)



2.2 Survey Metrics

At the onset of the operation, all systems were powered and calibrated prior to departure to ensure their operability and performance. Separate checks were completed for the GNSS, INS, MBES, and SeaScout

SAS systems. Upon proper calibration and alignment of systems, additional on-water tests were performed to verify the onboard sensors and verify the USBL. With the validation from these checks, the systems were deemed operationally ready, and the survey commenced.

Due to the weather forecast, it was decided to initially survey the BIWF site because of its likelihood of having more adverse environmental conditions that would prevent survey operations at a later date. Upon conclusion of that site, the vessel transited back into the LIS in more sheltered waters to deploy and survey the simulated targets.

2.2.5 Current Methodology

The primary survey system utilized for this project was the ThayerMahan SeaScout. With an onboard SAS and multibeam system, the platform allows for the simultaneous collection of multiple types of seabed data. Historically, most towed systems are SSS platforms. SSS systems are towed aft of the vessel and produce fan shaped acoustic pulses that are repeatedly emitted to the seafloor out either side of the towbody. A series of swaths are collected while that can be combined to produce an ‘image’ of the seafloor. SSS towfish can operate at a variety of frequencies and ranges, however, it is typical that there is a loss in the imagery resolution as a function of range, particularly in the along-track axis. SSS equipment can be used for a variety of reasons besides analyzing the status of cables. The data gathered from SSS equipment can be used for creating and updating nautical charts, detection of underwater objects, and identification of bathymetric features. SSS data is often acquired along with bathymetric soundings and other systems such as sub-bottom profilers to provide further insight on the structure of the seabed.

Bathymetric data is commonly collected with multi-beam echo sounders (MBES), and these are often hull or pole mounted systems. These systems can determine the depth of water under the transducer based on the velocity of sound through water, and the time from transmission to reception. They are useful when mapping large areas because the across track data coverage can be greater than three times the water depth. The vertical resolution of the depth data can be at the centimeter level. MBES surveys are completed prior to the installation of subsea cables as well as periodically after installment to provide details on water depths, seabed topography, cable burial status, and hazardous debris near cable runs.

Depending on the system used, typical side scan systems are limited by the across-track range due to resolution and frequency limitations. A SSS at optimal resolution can be capped close to 100m which limits the ACR to about 0.43 kilometers squared per hour (km^2/hr). MBES surveys will have a variable ACR due to their dependency on frequency and altitude. For a good comparison, the R2Sonic Sonic 2024

was utilized in this project to provide a comparative baseline to the SAS system. The estimated ACR for both systems can be seen in the following section.

2.2.6 Area Coverage

In surveying the cable corridor, the vessel covered 130 kilometers and gathered approximately 26.76 km² of seabed imagery. The corridor survey collected approximately 4.9 terabytes (TB) of data, 90% of which is associated directly to the SAS imagery. The remaining data includes the integrated multibeam dataset, environmental data, and system metadata. Using the cable corridor as a reference, the system's relevant ACR for this event was 1.9 km²/hr. It should be noted that the corridor survey was not performed at the optimal altitude or speed to maximize the system's area coverage. Due to the environmental conditions and the thermal gradient experienced at the time, the system was operated at a shallower altitude and slower speed as to maximize data quality. By comparison, SSS and MBES data of equivalent line km, acquired and processed at industry standard specifications, totals around 0.03 TB for MBES XYZ data, MBES RGB images, SSS data files and SSS mosaics. It should be noted that the file sizes are significantly greater for the SAS system due to the enhanced resolution of the system. Personal communications indicate that the problem of data storage is common across the European wind farm sector however, wind farm operators can utilize subcontractors or third parties for data storage facilities to alleviate this issue. GIS deliverables, such as GeoTiff images of mosaics; event listings and shapefiles etc. can often be used for post survey route engineering, resulting in much smaller requirements for data storage).

2.2.7 Reporting Requirements

Per the Agreement 115 SOW, the data products varied depending on analysis and desired use. File types included spreadsheets, GeoTiffs, text, charts, graphs, etc. As each processing software generates different file types, various formats were included as part of the overall data package.

In order to provide the hydrographic data set, all systems utilized in the survey were calibrated and verified prior to operation. Relevant system calibration and validation reports are included in Appendix A.

2.2.8 Data Processing

In order to help visualize the data and to fulfill cable failure task 4, mosaics were created of the SAS imagery. These mosaics were compiled and compared to historical imagery from previous surveys of the BIWF. The mosaics were created in the Teledyne CARIS HIPS and SIPS software by compiling the sonar

data and generating the output csar and tif files. Along with the generation of the mosaics, depth surfaces were generated from the collected bathymetry utilizing SeaScout's MBES and the R2Sonic 2024.

Additional processing was performed to re-beamform the SAS data to correct for excessive gyro movement as well as updated environmental parameters. This processing was completed using the Kraken Insight software which produces TIL files from the raw data files generated during the survey.

3 Data Review

The surveys successfully collected high-resolution SAS imagery of existing subsea infrastructure and simulated cable targets. The BIWF provided an in-situ real world baseline for imagery of turbine foundations, cables, mattressing, and cable crossings. These are further detailed in Section 3.2 Imagery Review, below.

3.1 Collection and Calibration

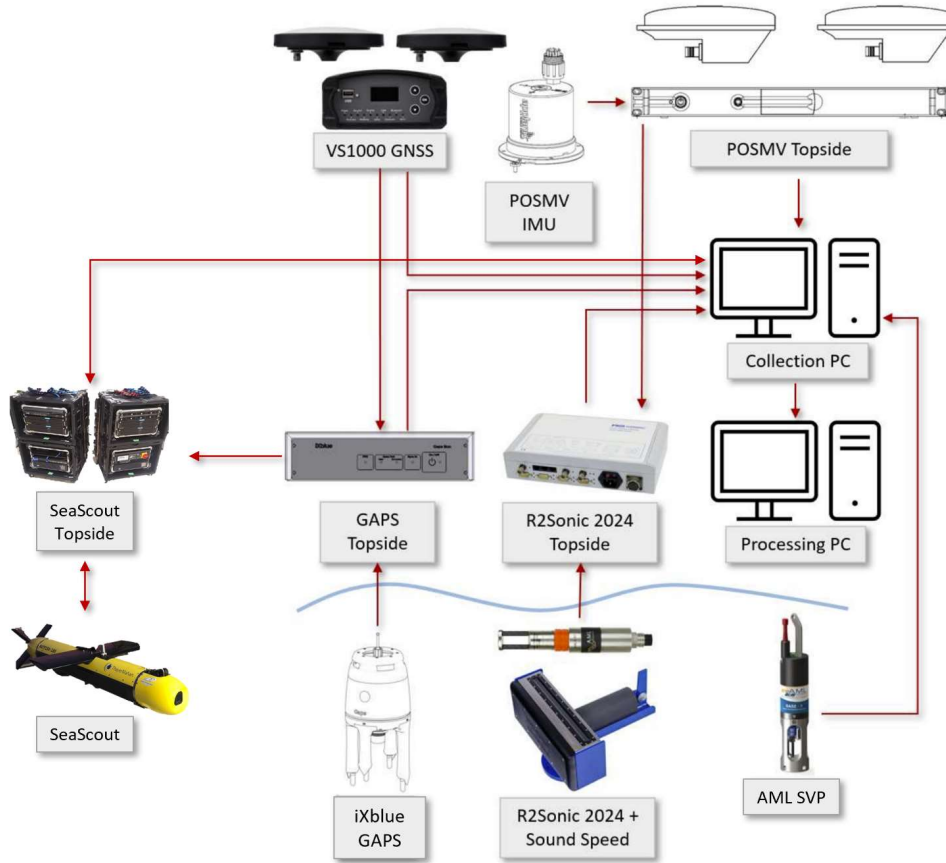
Survey lines were collected at various spacings in order to accommodate varied altitudes. In general, the altitude of the SeaScout was kept consistent throughout the survey at 15 meters. This altitude varied some to avoid lensing due to thermoclines or sound velocity stratification. The planned altitude was generally determined prior to deployment using data from the Sound Velocity Profiler (SVP) to inform of any large deviations in the water column. Also, due to the real-time feed of the SAS, any perturbation in the water column would be immediately realized in the imagery which allows for real-time corrections of altitude to avoid them. For the simulated target imagery, the altitude and range on the targets was varied in order to generate a dataset of varied angles and shadows of the targets for further analysis utilizing ThayerMahan's automatic target recognition (ATR) algorithm.

The sensors integrated on the *Berto Miller* were installed, calibrated, and verified with multiple tests to ensure functionality and geospatial accuracy. The GNSS and INS setup is different for the SAS and the R2Sonic multibeam such that they are running two completely different systems which each require separate tests and calibrations. The sensor interfaces and data workflow can be seen in Figure 5 below. The individual calibrations and certifications can be seen in the Appendix of this document.

Figure 5. Sensor Workflow.

Equipment integration workflow and data interfaces.

(Miller's Launch, Inc.)



3.1.1 SAS

The SeaScout system’s SAS utilizes positioning from its onboard INS aided by USBL positioning. To ensure the greatest accuracy for the system, offsets are measured between the vehicle, USBL, and primary GNSS. These offsets are applied within the systems and used to accurately orient the SAS data geospatially.

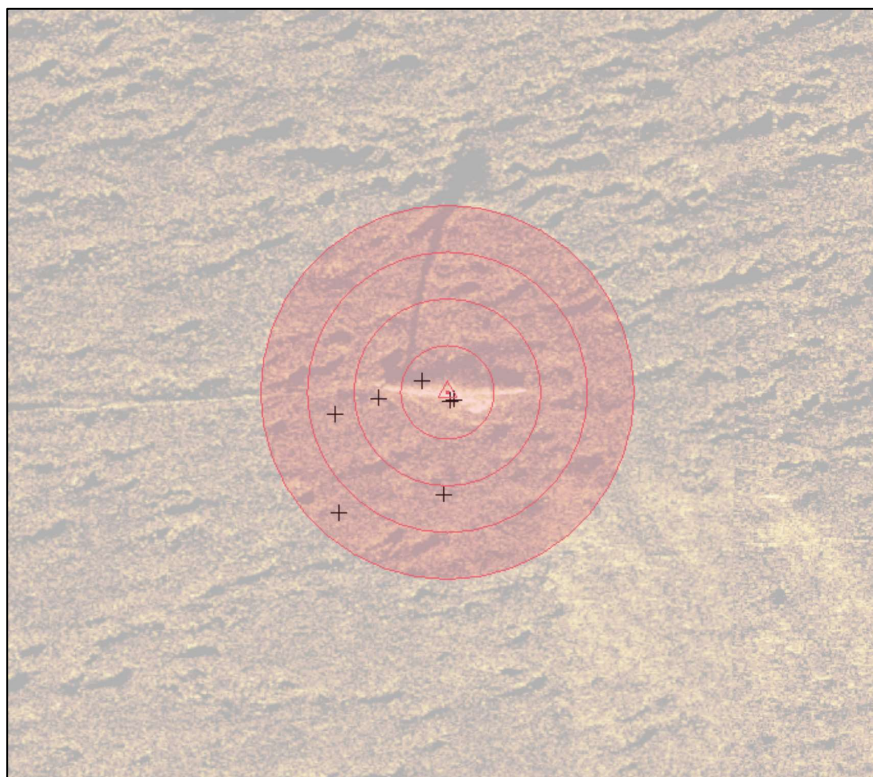
Based upon the collected data during the at-sea survey, the SAS imagery has a nominal positional accuracy of +/- 0.64m. This was determined by performing an Error Verification Test (EVT) analysis of the data collected within the simulated target deployment area, Figure 6. This analysis evaluates the

positional accuracy of the SAS by comparing static objects on the seafloor between subsequent passes of the object at varied angles and directions. Utilizing Target D in the aforementioned dataset the standard deviation was estimated at 0.43m.

Figure 6. Target D EVT.

Sampled target points with one meter range rings (Note: not centered on average).

(ThayerMahan, Inc.)



The EVT was performed for both sonar arrays with each data point representing a line transit running North-South, South-North, East-West, and West-East. Each array was also isolated and compared with the Port array averaging +/- 0.75m and the Starboard array averaging +/- 0.53m.

3.1.2 Multibeam

During the survey, multibeam data were collected simultaneously with the SeaScout’s integrated Norbit WBMS and the pole mounted R2Sonic MBES. Due to the location of the towfish (towed along the centerline) and the pole mounted multibeam (port of centerline), the coverage between the two systems

was offset along survey lines. Multiple lines were performed to help develop full coverage and target overlap. The R2Sonic multibeam serve as a control system for system comparison.

3.1.2.1 SeaScout Norbit WBMS

SeaScout's onboard multibeam is a Norbit WBMS. This multibeam was operated at a nominal frequency of 400 kilohertz (kHz) and uses a frequency modulated (FM) pulse. The ping rate was around 20 hertz (Hz), and the sensor configurations were able to be modified throughout the survey if necessary. The sensor was calibrated within the SeaScout, and the system generated standard s7k files, which included the inertial positioning and attitude data along with the beam geometry.

3.1.2.2 R2Sonic Sonic 2024

The Sonic 2024 is a MBES that can provide high resolution bathymetry. It has a selectable frequency range between 170-450 kHz and uses a continuous wave (CW) pulse. The R2Sonic was affixed to a dual mount frame along with the IXBlue GAPS M7 USBL as seen in Figure 7. Because the over-side pole was not initially configured for high-speed MBES surveying (> 4 knots (kt)) and had a deeper draft, at the SeaScout's operational speed (6-8 kts) the multibeam was susceptible to pole motion and possible water cavitation. These effects can create motion artifacts in the multibeam data. As an externally integrated system (not internally calibrated with platform prior to operations), the R2Sonic was dimensionally calibrated with the vessel reference frame. To determine angular mounting offsets, a patch test was performed. The results of this test can be seen in Appendix A.

Figure 7. USBL and Multibeam Dual Mount.

Sonic 2024 multibeam(left) and GAPS USBL (right) attached to dual mount port-side pole. Image is rotated 90degrees to show orientation of systems while in water, left would be bow forward.

(ThayerMahan, Inc.)



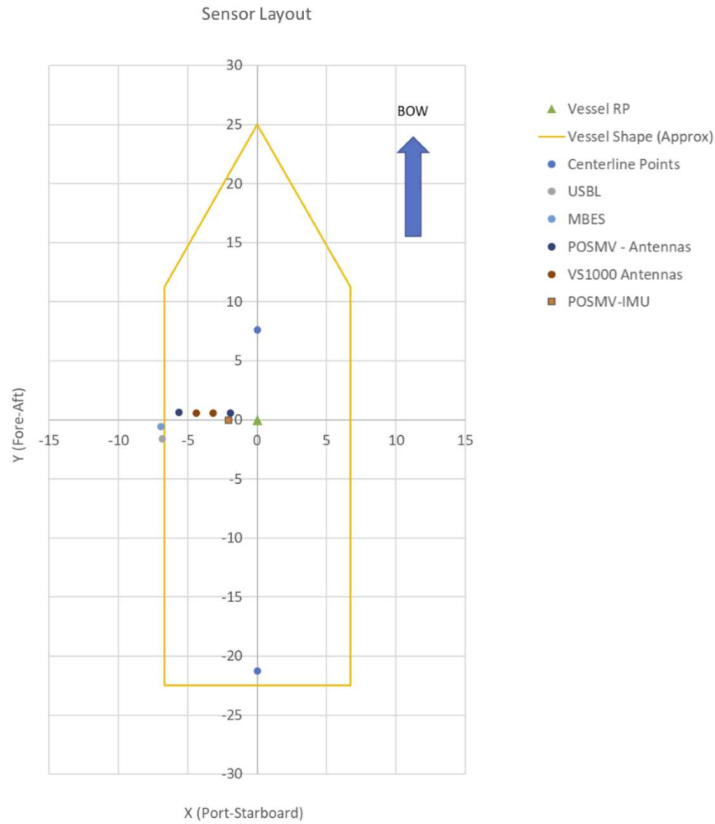
3.1.3 GNSS/USBL

The positioning for the SAS and Norbit multibeam were derived from the GAPS INS and USBL setup. The positioning for the inertial system was input from a Hemisphere VS1000 which utilized ATLAS correctors. The R2Sonic was setup differently using the onboard POS MV inertial setup with MarineStar correctors. These systems were installed on the vessel and fixed into position. The geospatial accuracies of these systems translate directly to the accuracy of the sonar data, so they were surveyed in during a dimensional control survey prior to the start of operations. The reference frame and targeted dimensions can be seen in Figure 8 below.

Figure 8. Vessel Reference Frame.

Dimensional control reported sensor positions.

(ThayerMahan, Inc.)



3.1.4 Laser Scanner

The SeaScout’s integrated SeaVision laser scanner is a full ocean depth profiler with both High-Definition camera and RGB laser. The profiler can perform live three-dimensional (3D) scans of seabed targets while integrated within the SeaScout towbody. The operational altitude needs to be lower (<8m) in order for the lasers to receive a positive return. Due to the lowered altitude, the SAS swath is reduced, so operational planning needs were considered when utilizing the scanner. The outputs of the scanner are LAZ files which allow for 3D point cloud mapping of targets.

3.2 Imagery Review

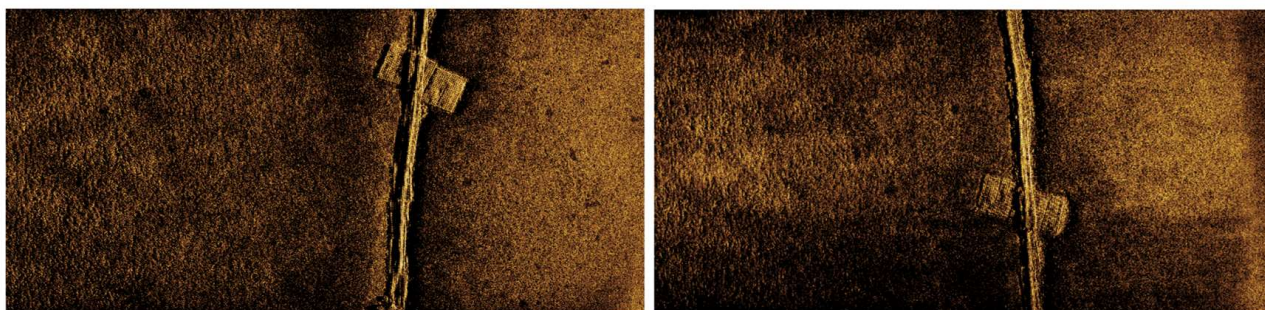
3.2.1 Existing Cable Routes

The imagery presented below was collected within the transmission cable corridor for the BIWF. This corridor runs from the offshore wind farm to the onshore station on Block Island and then back out across the sound to Narragansett making landfall near Point Judith, Rhode Island. The corridor is mostly buried but it is possible to see evidence of mattresses and trenching along its path. This is most obviously seen in the cable crossings in the corridor’s midspan. There are multiple distinct crossings, as seen in Figure 9, and a fourth that is less evident.

Figure 9. BIWF SAS Cable Crossings and Mattressing.

Various SAS images of BIWF cable crossings.

(ThayerMahan, Inc.)



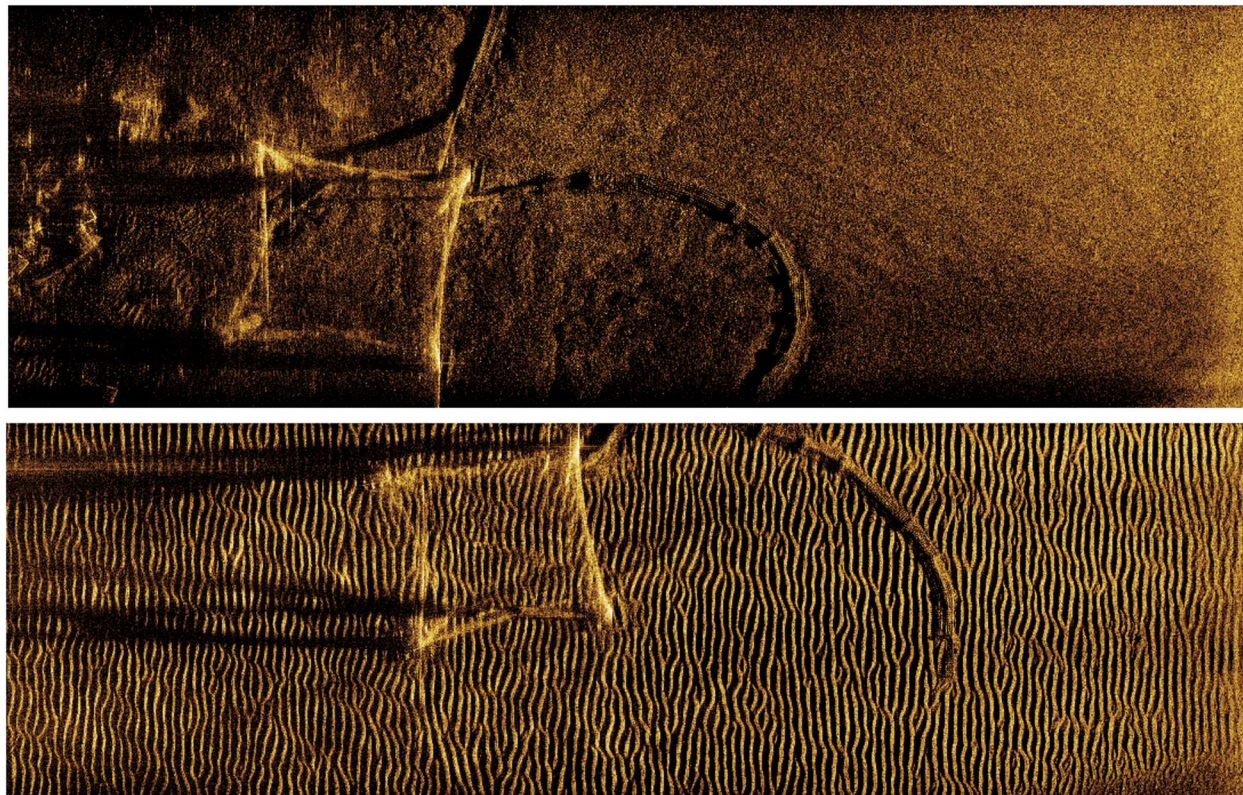
3.2.2 Existing Infrastructure

To further build a cable dataset and assess the condition of supporting infrastructure, the foundations of the BIWF turbines were imaged with SAS. In the imagery, Figure 10, it is possible to see the bases of the jacket foundation as well as some of the trusses. Along with the structure, the cable approach can be identified coming towards the foundation with the J-tube evidenced by its shadow. The cable mattresses is also apparent in these images as well as the surrounding environment. Between the five foundations imaged, different seabed types and environments can be seen. Varying sand waves, scour, and debris can be distinguished and characterized from one foundation to the next.

Figure 10. BIWF Wind Turbine Foundations.

SAS images of multiple BIWF wind turbine foundations.

(ThayerMahan, Inc.)



3.2.3 Environmental Hazards

Throughout the survey there were multiple examples of subsea hazards that are representative of potential failure modes for subsea infrastructure. In general, one of largest influences on subsea infrastructure is the surrounding environment. The presence of hard geology, from rock outcrops, coral beds, dense boulder fields etc., places limitations on cable installation. An important aspect of cable route design, engineering, and security is the shallow geological conditions along the route including the sediment properties, relative strength, and thickness which all influence the depth to which the cable can be buried and the effectiveness of burial as a protection mechanism. Areas of hard geology such as rock outcrops, coral, and dense boulder fields can cause a potential risk to the cable security due to the risk of abrasion, suspension, and exposure. Cable suspensions and exposure on the seabed also increase the risk of damage from fishing gear and anchor damage, as well as chafing on the rock itself.

The presence of strong currents can also have a significant impact on the abrasive potential of a cable route in areas where the cable is surface laid or has limited burial. Likewise, tropical storms, hurricanes, and cyclones, and significant storms can all also be a cause of cable abrasion in shallow waters.

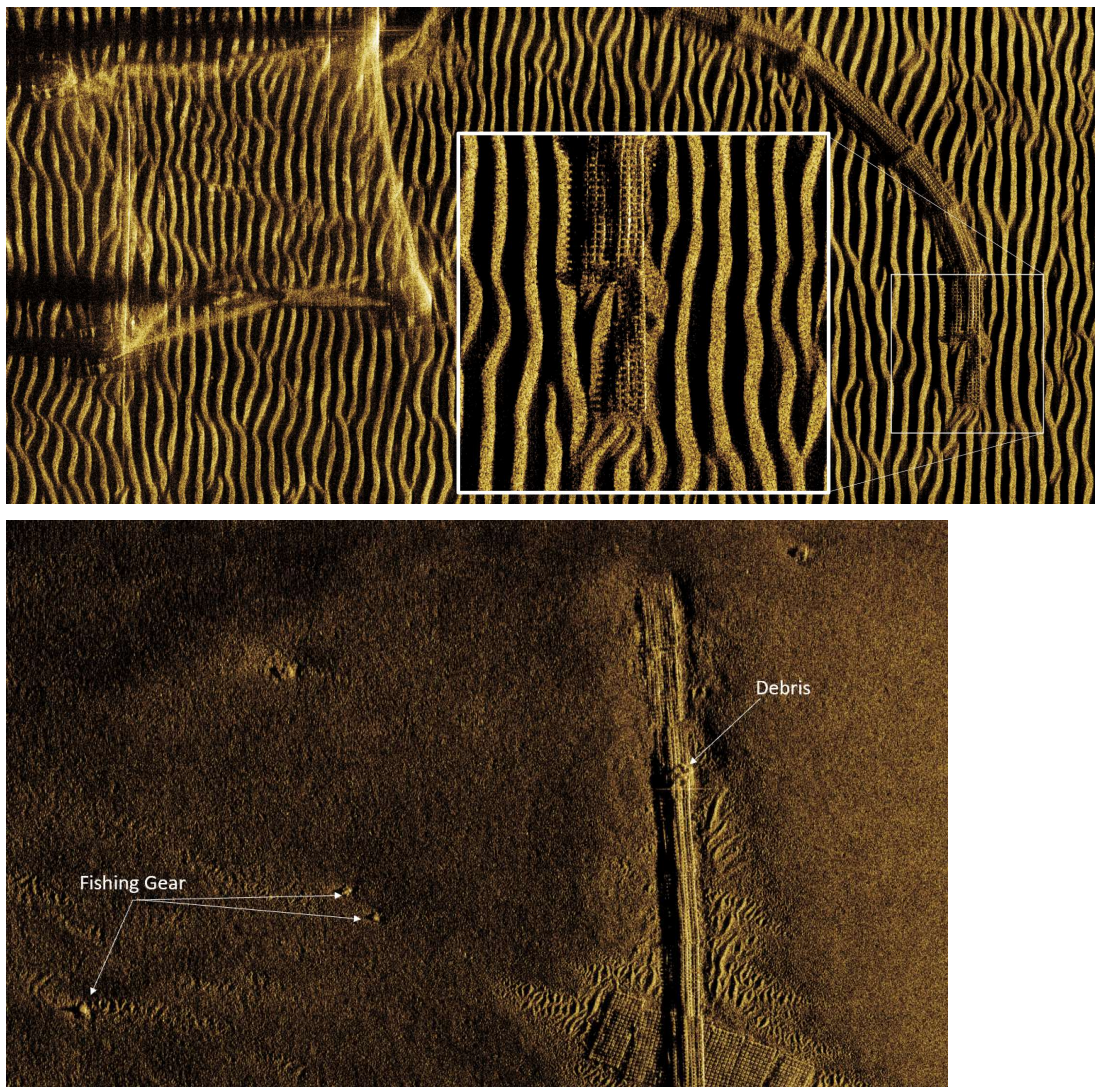
Along with natural influences, human-made hazards also pose a potential threat to subsea infrastructure. There is a high correlation between ecological impact on the seafloor by fishing gear types and impact on submarine cables, especially if the cable is exposed on the seafloor or only shallow buried. Evidence of past bottom trawl fishing and shellfish dredging activities can be preserved as seabed scars in fine and granular sediments which can often be noted in multibeam, side scan sonar, and SAS data. The potential for fishing activities is also a consideration in areas of mobile seabed. The presence of sand waves implies a dynamic seabed environment, and the movement of these sand waves can potentially cause cable suspensions in the troughs, which can be more susceptible to fishing activity.

In the cable corridor survey, there was no evidence of damaged cable, although environmental and human-made influences were present. As seen in Figure 11, the two photos show drastically different bottom-types. The top image visualizes the sand waves created by a high current area and how the sediment can shift. In this case, the shifting sediment has further buried the cable mattresses. In the lower image there is evidence of human-made influences on the seafloor. With fishing gear and debris in the vicinity of the cable route, there is evidence of commercial fishing in the area which can pose a risk to the infrastructure. It is also possible to see the scouring effect caused by the emplaced mattresses with sand waves forming around the edges of the structures.

Figure 11. Hazards Around Infrastructure and Cables.

SAS images of environmental and human-made hazards around existing infrastructure. Burial of cable mattressing around WTG (Top). Fishing gear and debris on and in the vicinity of existing cable mattressing (Bottom).

(ThayerMahan, Inc.)



3.2.4 Simulated Targets

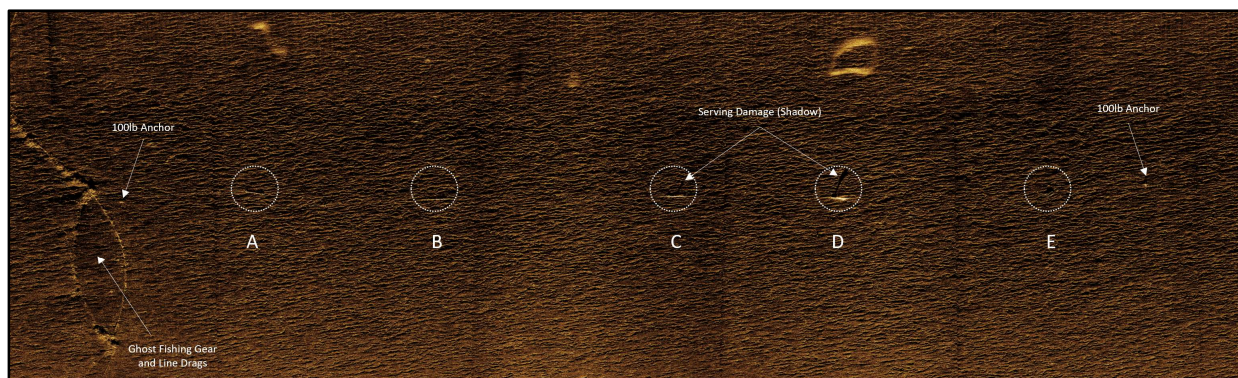
Along with the existing seabed infrastructure, the simulated targets helped provide references for the assessment of cable damage. These targets, labelled A-E, were prepared in order of increasing failure modalities to represent the effects of damages due to anchor drags, environmental effects, fishing gear, etc. These targets were rigged in a continuous line to allow for multiple passes to be performed at nadir,

near-field, mid-field, and far-field ranges of the SAS swath. SAS imagery of the continuous deployed target string, Figure 12, can be seen below.

Figure 12. SAS Continuous Target Image.

Cable targets A through E deployed in LIS.

(ThayerMahan, Inc.)



The condition and identification of the targets can be determined based on the intensity return of the SAS as well as with the respective shadows of the targets. For example, as seen in Figure 14, in targets C and D it is possible to see the shadow cast by the serving damage. This is further exemplified in comparison to the undamaged target A where the rectangular shadow accurately reflects the expected shape of the cable. In general, the increased damage (exposure of the cable armoring and serving material), results in a more intense and brighter return in the imagery.

From the imagery in Figure 12 it is possible to observe that the increase in cable damage is generally proportional to the intensity return. The table below outlines the maximum intensity returns. These values were queried at the mid-span of the cable (where the simulated damage is most prevalent) and their maximum values were returned. With the more damaged cables there is a significant increase in intensity return. This was consistent along passes where a higher intensity was attributed to the more damaged cables. It should be noted that the intensity can be affected by data quality and artifacts inflicted due to excessive vehicle motion or thermoclines. For example, on line 2022-04-25T21-25-17, the intensity reading for target B is suspected to be affected by excessive vehicle motion as evidenced in the imagery of that line.

Table 1. Comparison of Target Intensity.

Cable target intensity measurements in CARIS. These values were sampled across three different sets of lines.

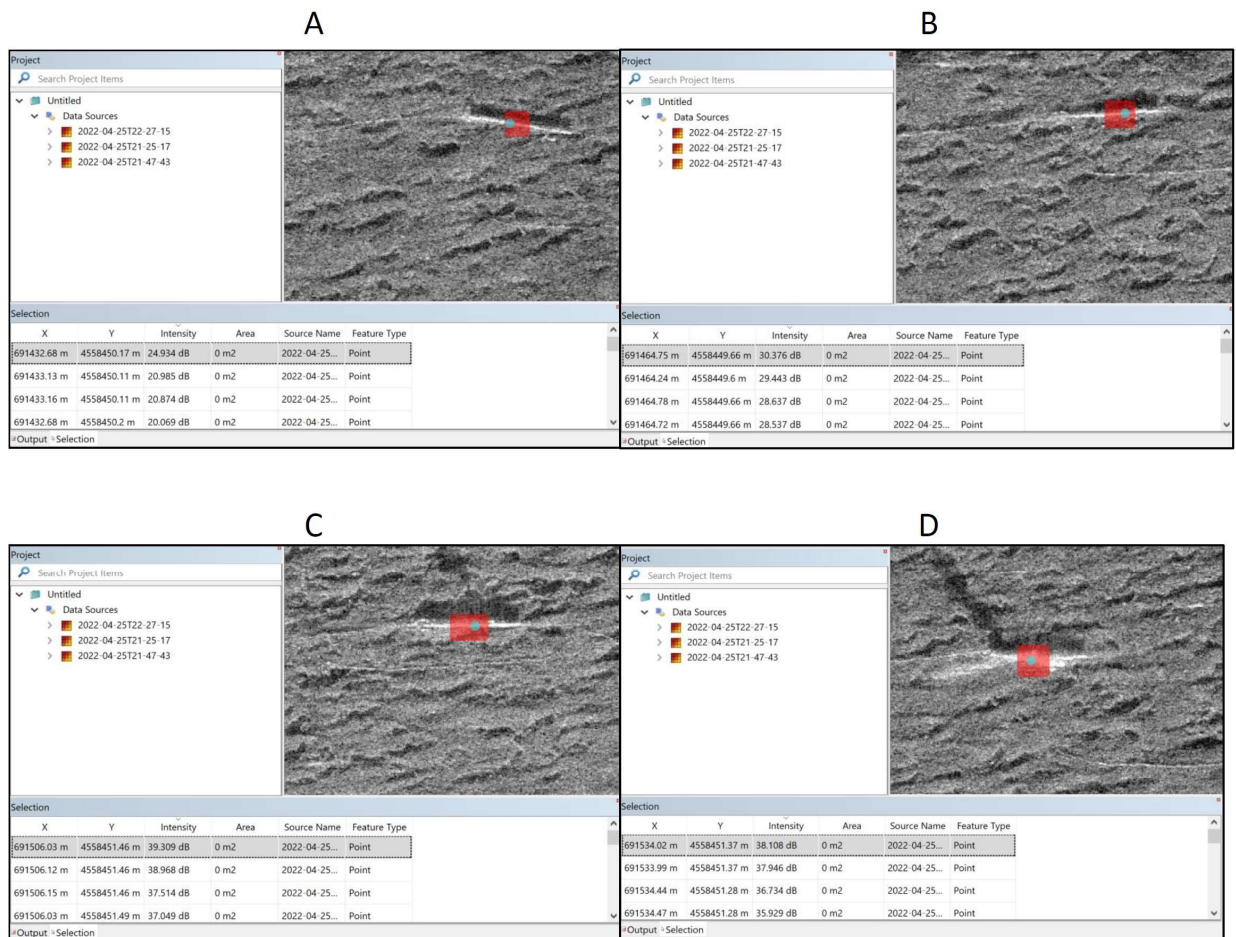
(ThayerMahan, Inc.)

Target Name / Average Intensity (dB)	A	B	C	D
2022-04-25T21-47-43	24.934	30.376	39.309	38.108
2022-04-25T21-25-17	22.663	21.779*	39.021	37.859
2022-04-25T22-27-15	26.905	33.127	38.640	41.178

Figure 13. Cable Target Intensity Comparison.

Cable target intensity measurements in CARIS. The central region was queried for the maximum intensity output (Represented by the green dot in each region).

(ThayerMahan, Inc.)

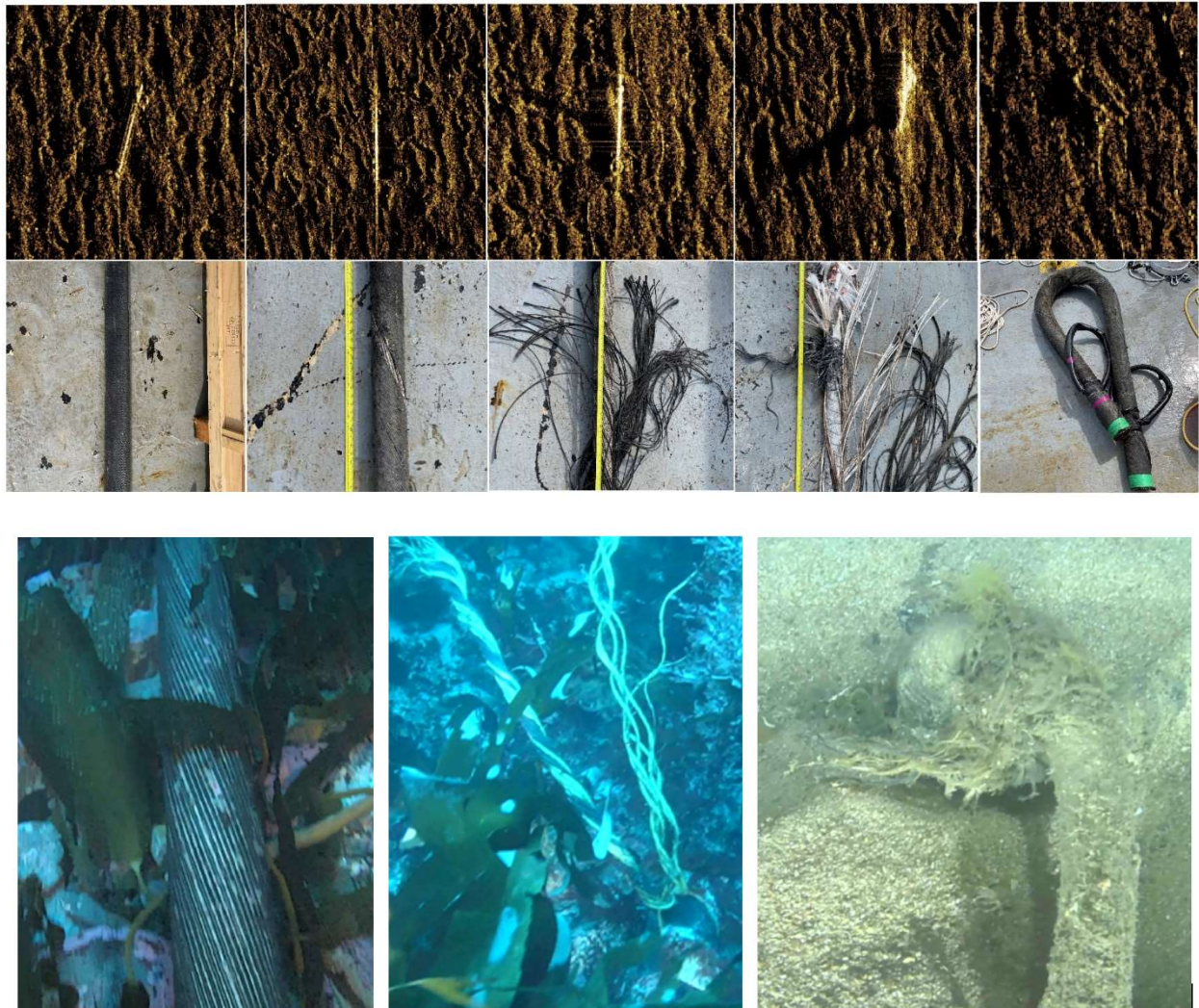


Future testing would ideally involve the use of additional targets with the goal to directly simulate a real-world exposure event. The simulated targets would ideally comprise longer sections (20-100m) of cable and varied degrees of burial for each. Each cable would then have some degree of damage along its length similarly to the executed event. Multiple passes would be collected and the ability to verify and elucidate the cable and its damage would be analyzed. Being able to have a normalized metric for quantifying damaged cable from the intensity return would add even more value to implementation of SAS as a cable monitoring tool. Not only would the system be able to visually decipher the existence of damage, but it could also provide insight to how damaged the cable actually is.

Figure 14. Cable Target Imagery Comparison.

Cable target prior to deployment on bottom, SAS image of emplaced cable target on top [A-E left to right]. Bottom images present typical remotely operated vehicle (ROV) imagery of typical forms of cable damage.

(ThayerMahan, Inc.)



3.3 Mosaics and Surfaces

The SAS mosaics for the survey areas were developed in the Caris HIPS/SIPS software suite. These mosaics are down sampled to 10cm resolution to make them easier to work with (due to file size). The benefit of these mosaics is that they provide a direct coverage comparison of the target area and can be referenced and overlaid with historical datasets to assess changes in the seabed. The additional benefit of building these mosaics is that they allow for layering and comparison with different data types.

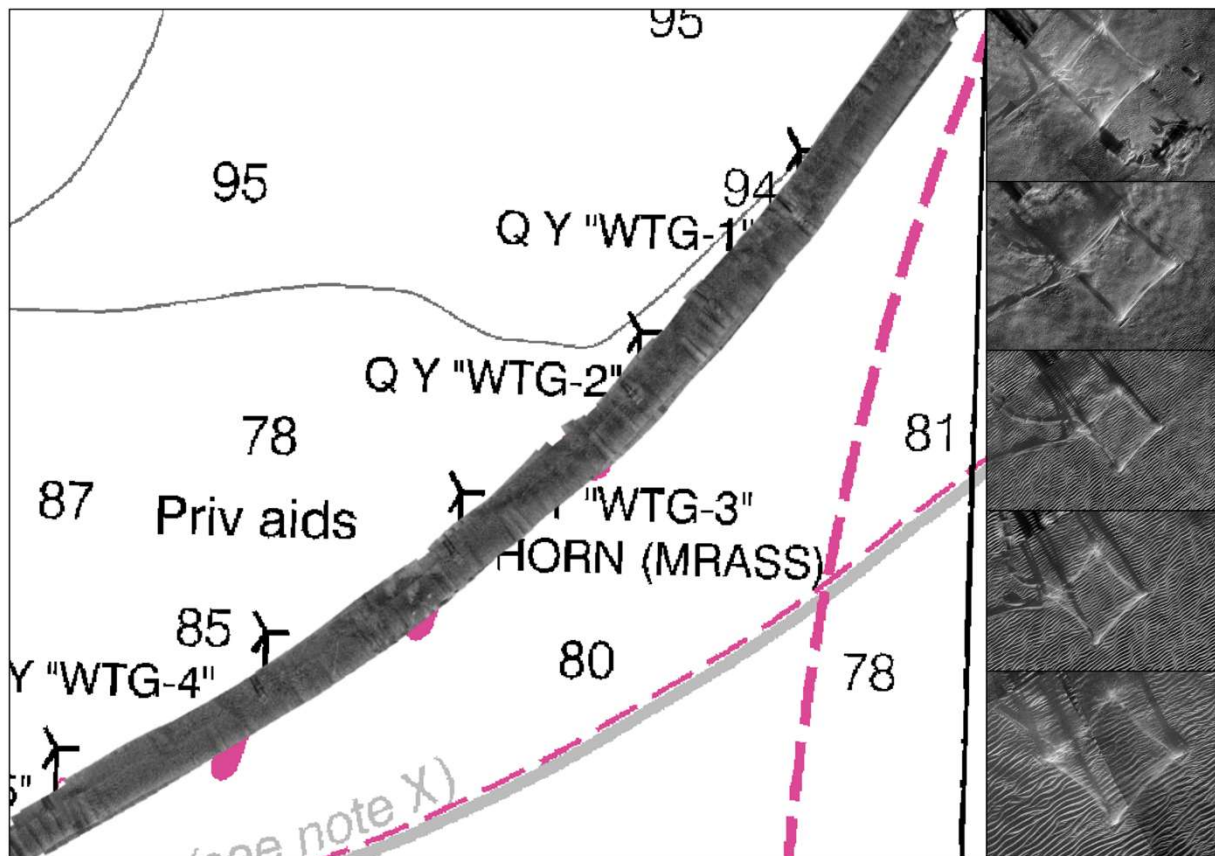
Bathymetric surfaces can be constructed and directly integrated with the mosaics to provide further characterization of the seabed.

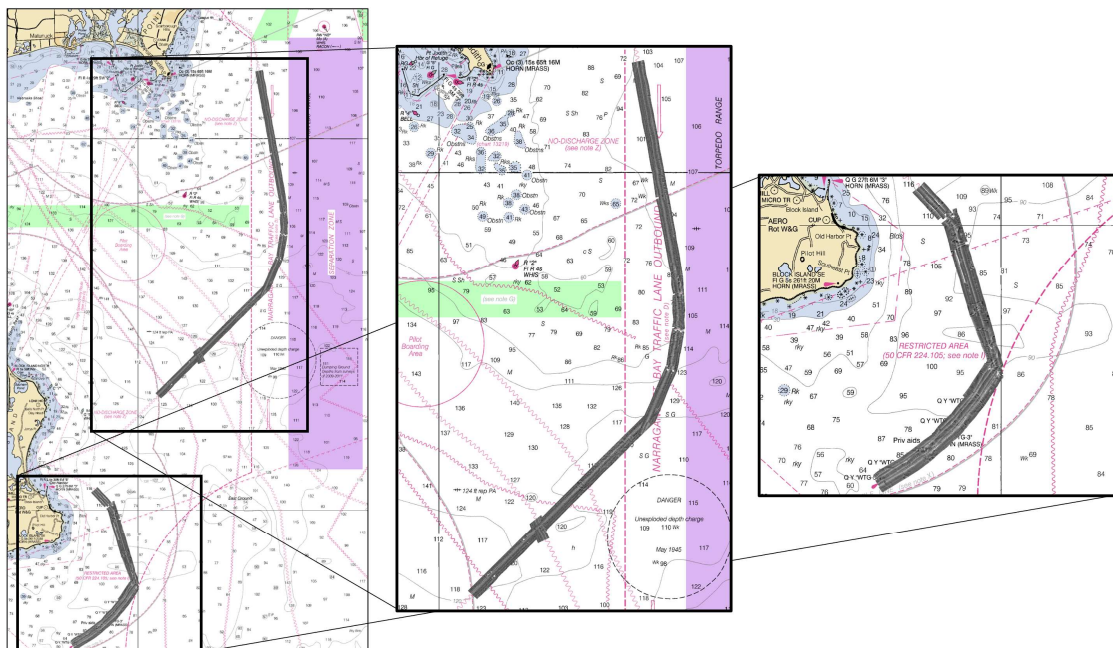
The mosaics for the BIWF inter-array cable corridor can be seen below, Figure 15. Within the mosaic it is easy to see where the foundation's feet are as well as the cable path to and from the turbine. It is also interesting to note that the seabed environment around each structure is slightly different. WTG 3, 4, and 5 all demonstrate an area of high current flow as evidenced by the predominance of sand waves around the structure. Some of the foundations also have debris near the base of the structures which can pose as future hazards. This is most easily visualized in the imagery of WTG-1 where debris has accumulated just southeast of the foundation where the burial for the export cable could potentially be.

Figure 15. BIWF Mosaic.

(Top) SAS imagery of the BIWF inter-array cables and WTG's. (Bottom) SAS imagery of BIWF cable corridor.

(ThayerMahan, Inc.)





3.4 System Engineering Analysis

Utilizing hydrographic software and post-processing techniques, it is possible to glean more information from the survey data. Utilizing metadata along with intensity returns and bathymetric readings it is possible to characterize targets of interest and their state. The SeaScout system performed well in the conditions of this survey with the imagery and positioning outperforming the initial system specifications.

A strength of the SeaScout system is its ability to rapidly collect simultaneous SAS and multibeam data. With the capability to survey at up to 8 knots, the system can theoretically achieve an ACR of 3 km²/hr. In comparison to autonomous systems, remotely operated vehicles (ROV's), and other towed sonars, this coverage rate provides a commercial benefit. Faster survey speeds and higher resolution imagery provide benefits for the surveys throughout the life cycle of a wind farm. Taking into consideration a direct comparison of side scan sonar (SSS) to SAS, most SSS can gather approximately 0.43 km²/hr under normal conditions, where SAS can practically collect up to 2.85 km²/hr. Equating this to collection rates, side scan costs approximately \$90 thousand per square kilometer, whereas the equivalent test at the SAS collection rate would be \$13.6 thousand per square kilometer. Note, this simplified comparison assumes equivalent rates for planning, mobilization, equipment, etc. This comparison is also solely for the application of SAS. When considering the additional sensors and future developments of the SeaScout system, the benefits become obvious.

There are still some limitations of the SAS system; some of which can be resolved with development and others which are inherent to the system. Since the SeaScout is a towed system, one of the limitations is its range in depth. Because of the coupling effects of vessel motion onto the fish and vessel wash, shallow water (<10m) environments can pose difficulty when attempting to survey. This motion can be translated from the vessel to the fish and could affect stability. On the other end of the depth range, the towbody is limited by the total amount of cable on its winch which currently limits the system to approximately 300m of depth. Adding more tow cable would be one solution but would also increase safety concerns for the vessel in way of physical limitations or potential snagging. Added cable also increases the required time for line-to-line turns which would reduce the operational coverage rate of the system. However, these limitations are not all too different than existing SSS and would be inherent of all towed systems.

3.4.1 Hardware Developments

One of the operational goals of this survey was to utilize the SeaScout's integrated laser scanner to develop three-dimensional point cloud models of the subsea cables. Multiple passes were taken directly over the simulated targets to build these datasets. As an optical imaging system, the laser is highly dependent on the clarity and turbidity of the water. In the case of this survey, there was a substantial degree of turbidity present which prevented the laser scanner from resolving the seafloor and the cables. Future improvements to this implementation would require operational planning to execute laser surveys during a slack tide and during periods of enhanced water clarity. Due to the nature of this survey to simultaneously collect SAS, multibeam, and laser imagery, there was limited operational flexibility to isolate an ideal window for laser scanning.

3.4.2 Software Developments

The primary output of the SeaScout SAS is the proprietary TIL data format. TILs are individual tiles of processed raw sonar data. These files utilize the Kraken INSIGHT software for processing. Due to the proprietary nature of the file format, there is limited commercial software that can work with the TILs. As of now the primary post-processing software is CARIS which allows for mosaicking of the individual files and exportation in various file formats that are more ingestible into external hydrographic software. For the most part, these files are output as GeoTiffs which are supported by most GIS-based software. Future software developments would require the integration of the TIL file into additional hydrographic software, granted this would be dependent on external support and greater industry acceptance of the file format.

Future analytical work will involve processing the datasets through an ATR software which will be able to identify and locate individual targets of interest within the data stream. Early integration of this has yielded promising results, but the robustness of the algorithm is directly proportional to the accuracy and size of the control dataset. As the base control set becomes better defined then the software can be trained to better identify targets in new datasets.

The application of ATR has many implications on the post-processing of sonar data, the most significant of which is the time efficiency. Being able to automatically tag datasets without multiple operators having to pick and characterize each target saves labor, time, and money. It also allows for rapid identification during preventative maintenance surveys which is imperative for highlighting failures and beginning repairs.

3.4.3 Change Analysis

In fulfillment of survey task 4, the detection of movement and change in the seabed over time was analyzed. This analysis was performed in two studies, pre/post retrieval of targets and historical comparison of cable corridor imagery. The first event provides the benefit of assessing an area of known change and determining the impact of the deployment and retrieval. The second event demonstrates the potential influence of environmental factors and temporal changes. Both events help demonstrate the benefit of routine high-resolution surveys and how they can act as preventative maintenance measures for cable monitoring.

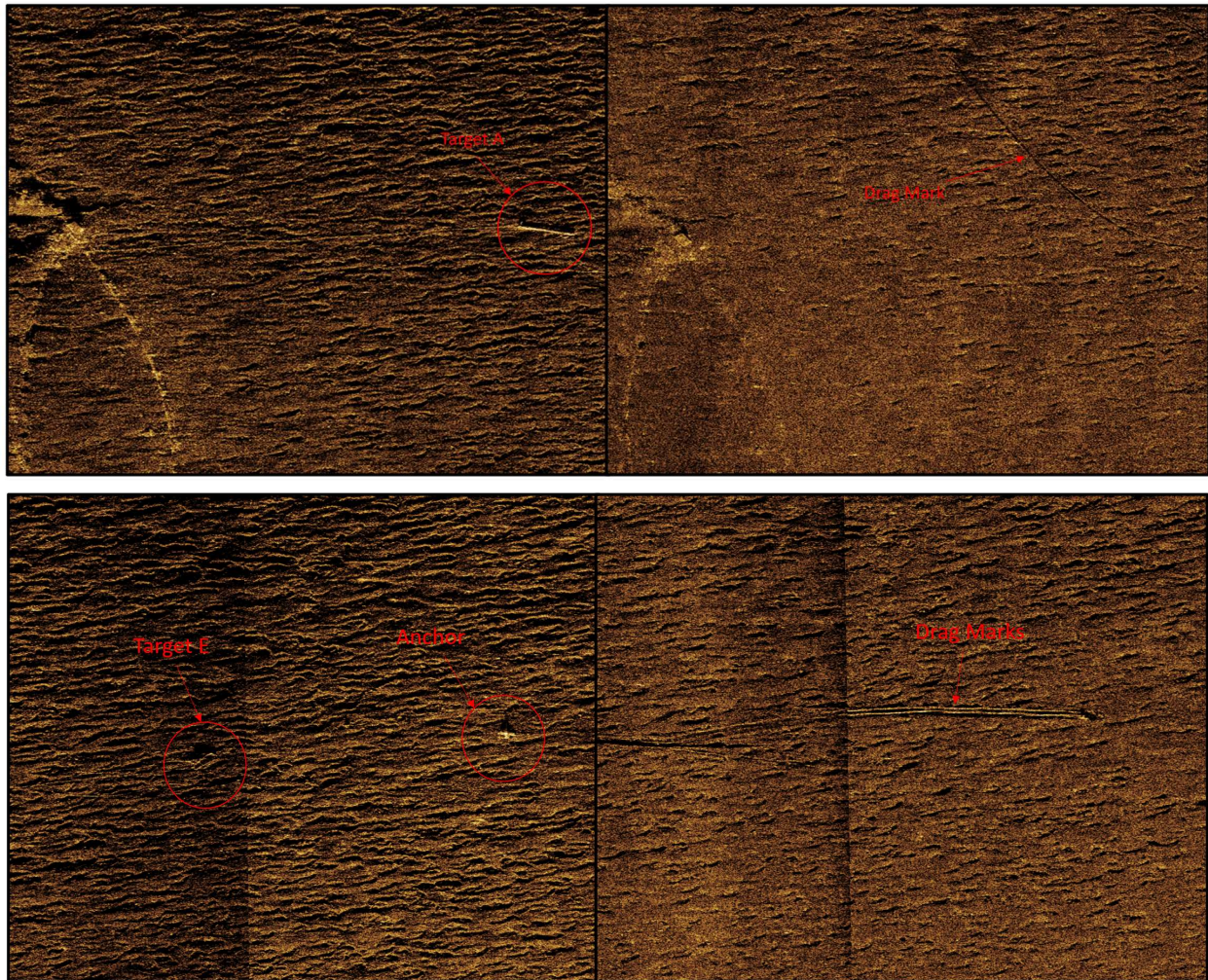
Target comparison study

The purpose of the target comparison was to emphasize the impact of emplacing and removing objects from the seafloor and how that is visualized using SAS imagery. Surveying the site after the targets were removed allowed for features such as drag marks and impact craters from when the simulated targets were deployed on the seafloor to be detected, as shown in Figure 16.

Figure 16. Simulated Target Post-Recovery SAS Comparison.

SAS Imagery of targets before and after recovery. Target A (top) and Target E (bottom)

(ThayerMahan, Inc.)



Historical analysis study

The largest takeaway from surveying the existing BIWF cable corridor is the ability to visualize potential environmental impacts in a real-world application in way of active cables. From prior surveys there are sections of cable that can be directly compared to the recent imagery.

When comparing to the historical baseline, there are various areas of obvious change, such as displaced objects and evidence of dredging (or lack thereof). In general, large environmental changes cannot be seen in such a short time frame comparison, but the evidence of dynamic environments is further confirmed through historical analysis. For example, previous areas of sand waves continue to show their

presence although their patterns have changed between years. Figure 17 demonstrates such an environment around one of the BIWF WTG’s.

Figure 17. Historical SAS Imagery Comparisons.

(Left) WTG foundation during the recent survey in 2022 (Right) WTG foundation from a SAS survey a couple years prior.

(ThayerMahan, Inc.)



3.4.4 Sensor Comparison

During the survey, three separate data sets were collected: the pole mounted R2Sonic MBES data, the towed Norbit MBES data, and the towed SAS data. Comparative samples of each data set were taken to demonstrate the capabilities of each system.

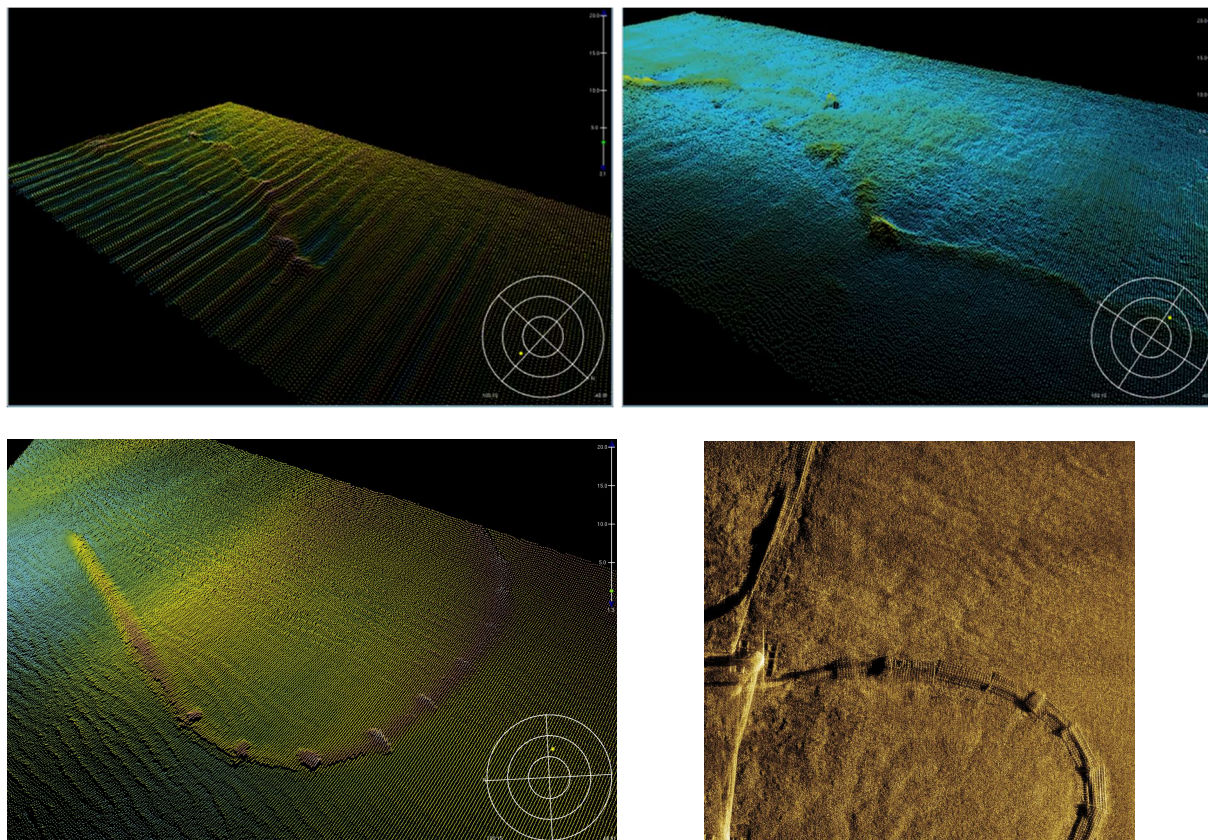
As seen in the R2Sonic point cloud in Figure 18, motion has translated into the data due to vibration in the pole mount. This is due to the survey speed exceeding the pole’s limitations. Comparatively, the Norbit MBES surface looks much smoother as it is integrated within the actively stabilized SeaScout platform and decoupled from the vessel and pole motion.

Between the SAS and the MBES data it is possible to see the benefits of the SAS’s horizontal resolution and the detail it shows along the cable run. With regards to visualization of damage, the MBES lacks the horizontal resolution to glean any details as to the state of the infrastructure. This is especially apparent when considering the bathymetric surfaces in way of the simulated targets. Where the SAS is able to detect and even differentiate the damage within the cable, it is difficult to visualize the cable itself within the MBES surface.

Figure 18. Bathymetric and SAS Imagery Comparisons.

(Top Row) Pole-mounted R2Sonic MBES data (Left) and towed Norbit MBES data (Right). (Bottom Row) Towed MBES bathymetry (Left) and SAS Imagery (Right) of WTG mattressing.

(ThayerMahan, Inc.)



3.5 Machine Learning/ATR

ThayerMahan, Inc.’s current ATR technology may be leveraged to accomplish the four cable failure tasks listed in Agreement 115. The current technology, trained on proprietary TIL tiled images and already in use, automatically detects and identifies blocks, lines, rocks, pots tires, wrecks, and natural and human-made entities within an input tiled image. Developing related technology to automatically detect and identify fishing gear, damaged cable, and cable and seabed movement is likely feasible, provided sufficient relevant and pre-labelled data to train the technology’s machine-learning architecture. A quality dataset is paramount for a dependable ATR system. ThayerMahan, Inc. is in a unique and strategically elevated position to implement such technology, given the SeaScout system and its ability to utilize the technical capabilities of the SAS system to capture an extensive and feature-rich dataset of images.

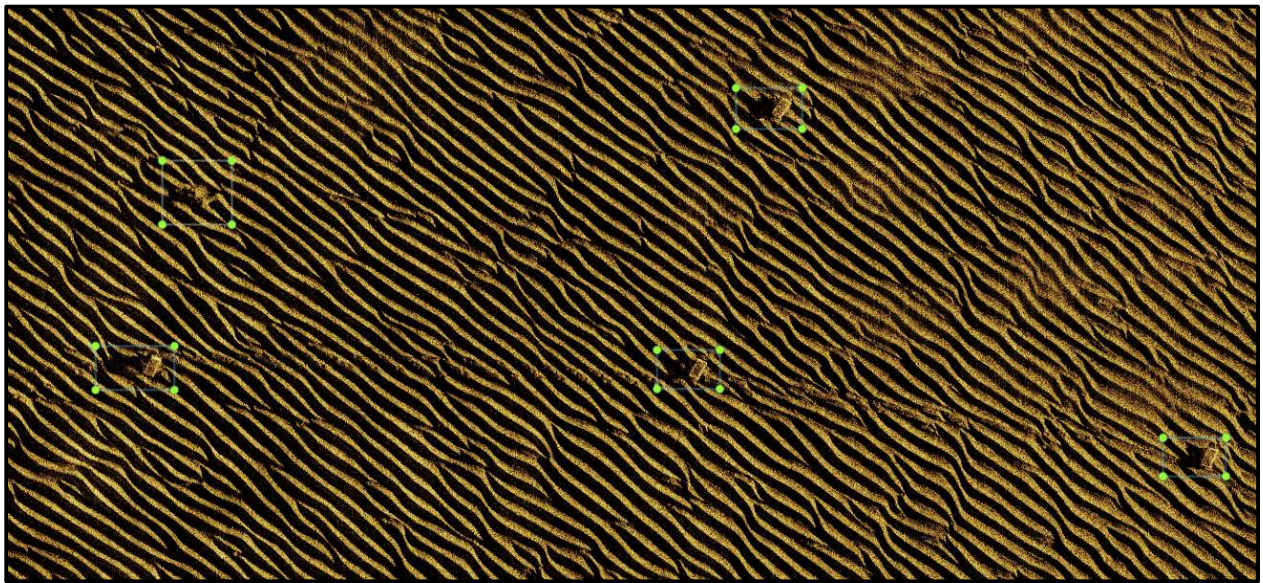
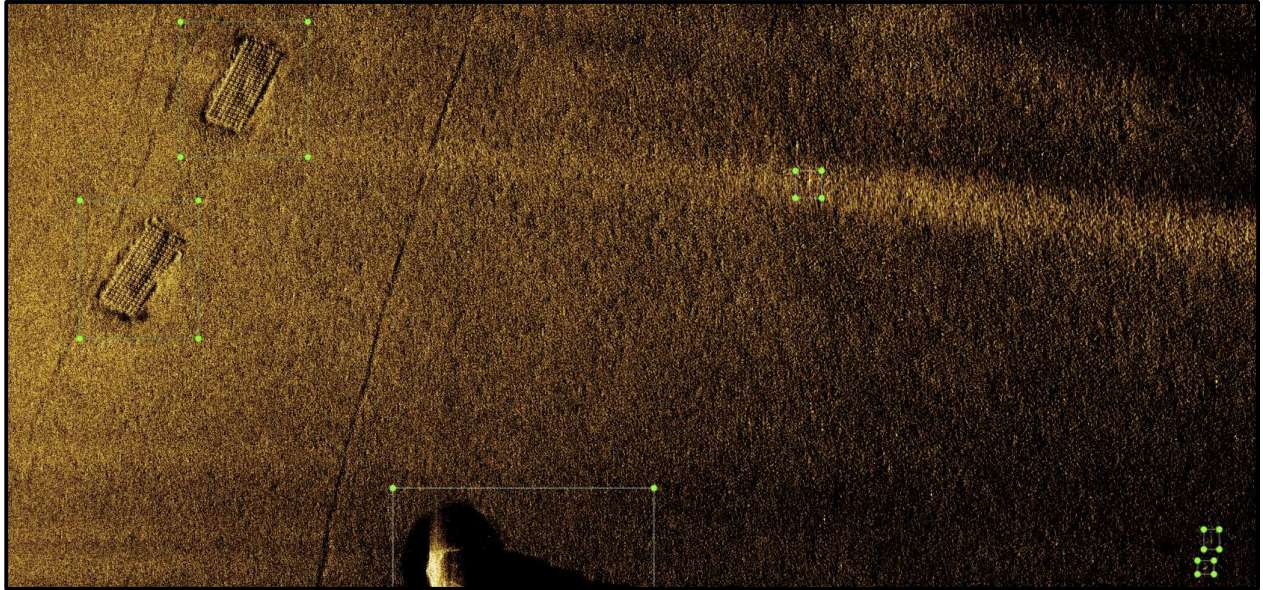
The cable target comparison in Figure 14 highlights the ability of SAS imagery to capture features that are indicative of cable damage and the severity thereof. Easily discernable to the eye, the modalities of targets A-D in the figure are easily discerned by a carefully designed ATR system trained on SAS imagery. Even target A with the least severe damage is discernable from the background, as shown in Figure 12. The U-shaped bend in target E, however, is more challenging for an ATR to detect, as this modality is difficult to discern even for the human eye.

An example output of ThayerMahan Inc's ATR system can be seen in Figure 19. As shown by the green bounding boxes, the system can detect discrete objects in the otherwise homogeneous seabed. In the top image, two cable mattresses along the BIWF cable corridor can be seen as well as a large boulder and its subsequent shadow near the bottom of the image. The lower image also shows the capability of the system to detect objects, likely derelict fishing gear, in a less homogeneous environment with the prominent sand waves throughout.

Figure 19. AI Tagged SAS Imagery.

Example SAS imagery with AI tagged annotations (as seen as bounding boxes).

(ThayerMahan, Inc.)



3.5.1 Current ATR Details

The current ATR technology in use at ThayerMahan, Inc. utilizes the machine-learning algorithm architecture known as You Only Look Once (YOLO). YOLO is a deep-learning architecture that can accept an image as input and return the location of object(s) of interest within the input image by

outputting a set of parameters describing a bounding box, one set of parameters for each object detected in the image. Conveniently, the algorithm is also capable of identifying the object contained in each bounding box using the same architecture. (i.e., it “only looks once” at the image for localization and identification functions). Because YOLO is a supervised learning algorithm, it requires manually labelling each input image used to train, validate, and test the algorithm, which consists of the set(s) of bounding box parameters and the identity of the object in the image. YOLO, during its training routine, learns the relationship between the desired outcome (bounding boxes, identification) and the images’ pixel values.

3.5.2 ATR Considerations

Repurposing the YOLO architecture to automatically detect and identify fishing gear and damaged cable (tasks 1, 4) is feasible and requires two steps. First, SAS images are manually annotated with the desired outcomes: bounding boxes surrounding the fishing gear and damaged cables, and the identity of the object within each box. Second, the YOLO architecture is retrained on these new YOLO-annotated files so that it learns the desired outcomes. Since these outcomes are similar to those already predicted by the current ATR technology, transfer learning concepts may be leveraged during the algorithm’s training and testing routines to keep computational effort to a minimum. Training is accomplished using the mean average precision (mAP) performance metric with a suitably chosen intersection-over-union (IoU) threshold for classification.

To ensure that machine-learning best practices are followed, testing is carried out on data previously unseen to the architecture during training. Accordingly, the YOLO-annotated dataset is randomly split into training and testing sets prior to training. The splitting-training-testing scheme is repeated a number of times (e.g., 5 or 10) such that each annotated data file is used as a testing point exactly once – a process called cross-validation. Reporting the performance on the test sets and aggregating or averaging them together provides an accurate measure of how the algorithm performs “in the wild” and ensures that no single anomalous testing dataset sabotages the results.

Before the images are served to the model for training, validation, and testing, ThayerMahan, Inc. utilizes a patented tiling technique to tile the original image into the required input size to satisfy hardware constraints. ATR algorithms, such as YOLO, requires images to be downscaled to a small size (e.g., 640x640). Our tiling technique adheres to the processing requirements for deep neural networks, which demands sufficient virtual memory (VRAM) to train the ATR model. The processing requirements of which scales logarithmically with the amount of input features (i.e. pixel resolution). Adhering to the limitations in this way drastically reduces the time required to train the algorithm, and otherwise makes

training possible. Since the data averages a native width and height of 5236x1544, downscaling the high-resolution imagery to a much smaller resolution degrades the features of the objects of interest to mere pixels, and thus prevents the model from correctly learning the features of each class.

3.5.3 ATR Preliminary Results

Using the tiling technique and YOLO architecture, we test the ability of the ATR system to classify tiled images as belonging to one of the five classes A through E, as in Figure 14. The dataset, which consists of 253 tiled images each manually annotated as A through E, is partitioned such that 70% (177 tiles), 20% (51 tiles), and 10% (25 tiles) of the tiles comprise a training, validation, and test set, respectively. Using the training set, the algorithm learns the relationship between the image pixels and the class labels. We fine-tune the algorithm's hyperparameters, specifically, the number of training epochs and the prediction confidence threshold, by observing its ability to predict the labels in the validation set. Finally, we evaluate the tuned algorithm's performance by observing its ability to classify the test set, which is comprised of tiles previously unseen by the algorithm.

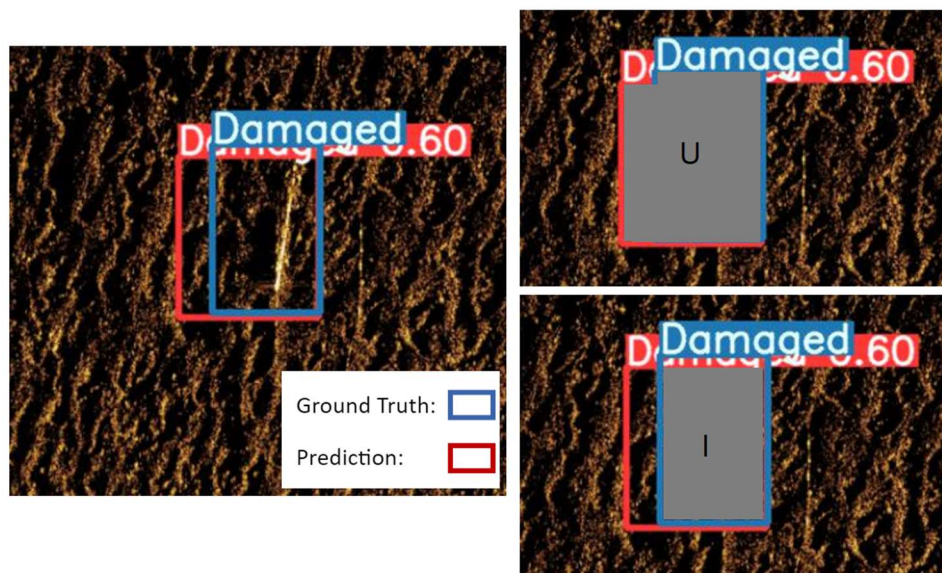
For the sake of comparison, and ease of interpretation for the images shown within this report, the classes A-E were collapsed into two classes (damaged and undamaged). This binary dataset variant was created to establish a baseline performance for our five-class model. The five-class model discussed in this section will be used in real world deployments of our ATR capabilities.

We use mAP with an IoU threshold of 50% as the performance metric for evaluation. A large mAP is preferred, and the maximum mAP value (100%) corresponds to the annotated ground truth matching the predicted model annotation 1:1. Figure 20 illustrates an example case for which the algorithm predicts a bounding box sharing an IoU of about 75% with the actual, manually labeled bounding box. The ratio of the boxes' overlapping area (the intersection, "I") to their total area (the union, "U") is about 0.75. The prediction is considered correct in the mAP calculation since the IoU is larger than 0.50.

Figure 20. Comparison of Actual and Predicted Annotations.

Comparison of actual (ground-truth) bounding box and that predicted by the ATR showing the union “U” and the intersection “I”.

(ThayerMahan, Inc.)



Additionally, we employ data augmentation in order to increase the number of tiles in the training set. Data augmentation, which is the process of expanding the dataset by engineering new images that are distorted versions of the originals, has been shown to increase classification performance when the original dataset is insufficient in size and the engineered images can provide useful information to the classifier. Accordingly, we expect this technique to improve performance for two reasons: (1) Our training dataset of 177 tiles is insufficient to properly train accurate deep-learning architectures such as YOLO (ideally, each class would be represented by 10,000 samples within a dataset in order to perform successfully on real-world data), and (2) select variations in the shapes of objects are likely to be encountered in practice and are therefore informative to the classifier. We distort the training tiles by reflecting them over the vertical axis – for example, a cable extending diagonally top-left to bottom-right in an original tile extends diagonally top-right to bottom-left in the engineered tile. The engineered tile, in this case, is informative since it is reasonable to encounter such a tile in practice. We apply this process to each tile in the training set to double its size. We do not augment the validation or test sets in order to maintain a realistic testing framework. Table 2 shows the number of tiles in each class before and after data augmentation.

Table 2. Number of Tiles in each of the Dataset Partitions, before and after Augmentation.

Tiles for each dataset, filtered by target class.

(ThayerMahan, Inc.)

Class	Training, Original	Training, Augmented	Validation	Test
Total	177	354	51	25
Class A	28	56	7	5
Class B	27	54	7	6
Class C	41	82	12	4
Class D	45	90	15	6
Class E	36	72	10	4

The optimal performance of our model configurations were models trained on the original data plus the augmented set. Evaluating the best algorithm trained on the aforementioned dataset produces a mAP score of 0.806 on the test set (out of a maximum possible score of 1), which is promising, considering the dataset is relatively small for training ATR systems, even with the engineered tiles. This score indicates a high true-positive rate and, at the same time, a small false-positive rate. We also consider the algorithm’s performance in the absence of the engineered tiles to better understand the efficacy of data augmentation and to motivate more augmentation in future tests should the results warrant it. Without data augmentation, we observe a reduced mAP score of 0.615, a difference of 0.191, and consequently may conclude that the data augmentation scheme greatly improves the classifier’s performance. With an increased sample size in our dataset in the future, we expect the model to perform significantly better across each class.

3.5.4 ATR Discussion, Analysis

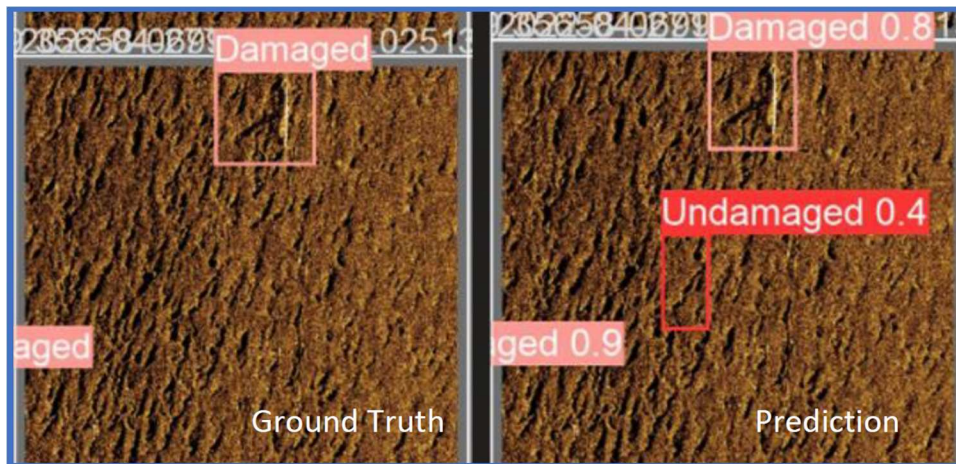
The tiling method coupled with the YOLO classifier performs well in identifying the linear patterns indicative of cable damage. When the algorithm does misclassify an object, it sometimes identifies a strong linear pattern in the background sea floor, yielding a false-positive prediction. This is observed in Figure 21, which indicates the ATR system incorrectly identifies a piece of the sea floor as an “undamaged” cable (i.e., Class A). As mentioned previously, the algorithm will more accurately discern cable from background when provided with more training data.

Augmenting the dataset greatly improves the classifier’s performance, and this fact suggests both that more training data will lead to additional increase in performance, and additional data augmentation techniques will provide useful information to the classifier. Training the classifier with enough real-world data is feasible given ThayerMahan, Inc.’s extensive dataset of SAS imagery, though the additional images will need manual labeling of the targets, which can become infeasible with very large datasets. If necessary, more data augmentation techniques such as reflecting over the horizontal axis, shearing, rotating – and the combinations therein – may be leveraged in order to circumvent the issue of manual labeling. Additionally, ThayerMahan Inc. is actively researching methods to synthetically generate SAS imagery to supplement existing datasets via simulation and general adversarial networks (GANs). Most likely, a combination of manual labeling of real-world images and programmatically engineering new images is optimal.

Figure 21. ATR False Identification.

Incorrect finding of an undamaged cable with the ATR.

(ThayerMahan, Inc.)



Provided in Figure 22, the confusion matrix gives the rate at which one class is predicted as another and is helpful in identifying individual classes that confuse the algorithm. Each column represents a true class, and each row, a predicted class. A diagonal matrix is ideal. From the matrix, Class D, with an accuracy of 100%, is the easiest class for the algorithm to discern. Inspection of Figure 14 makes it clear as to why Class D is so easy for the ATR to identify: As the class representing cables with the most damage, Class D images each contain an obvious intense bright spot indicative of the damage. Class C, by similar logic, should be easy to identify as well; however, the matrix indicates only a 25% success rate. Recent human

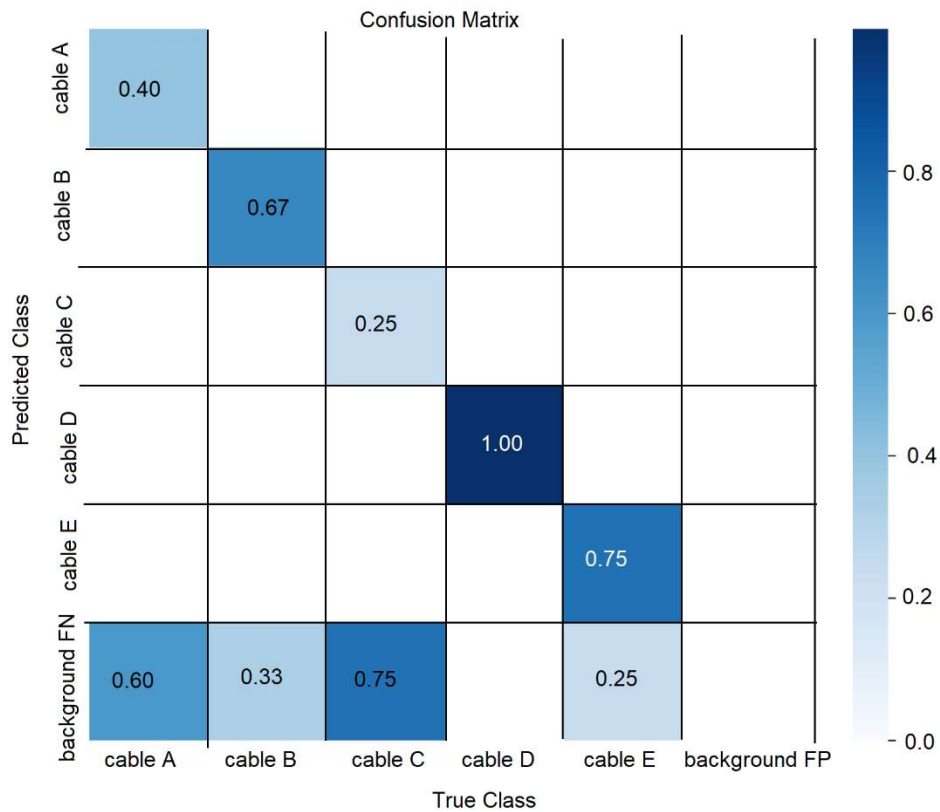
inspection of Class C images reveals human error of improperly annotated bounding boxes, which we will soon correct and re-test. In future research conducted on the dataset, ThayerMahan Inc. would like to observe model performance when the objects annotated as Class C are reannotated as either Class B or D, thus creating a four-class set. Proceeding down the diagonal of the matrix from the top-left, but ignoring Class C, the accuracy increases up to, and including Class D, and then decreases with Class E. This agrees with Figure 14, where it is observed that the damage-indicating brightness intensifies until Class E, which is more difficult to discern. From the matrix we also learn when Classes A, B, and E are misclassified, they are always misclassified as background.

These preliminary results are encouraging, but additional testing with greater number of data points is required. As indicated in Table 2, only 25 tiles were tested, with no more than six tiles in any single class. It may be the case that these tiles were easy, or obvious, for the algorithm to classify. More real-world images of each class are needed to populate the test set in order to better estimate the performance of the algorithm in real-world situations. Moreover, testing must be conducted on more than one test set, as it could be the case that one single test set happens to be anomalous. Once more data are collected and annotated, a five-fold cross-validation scheme may be employed to guard against the anomaly issue and provide a more realistic performance metric.

Figure 22. Confusion Matrix of ATR Performance.

From the test set, a confusion matrix was developed to analyze the ATR performance.

(ThayerMahan, Inc.)



3.5.5 ATR Development

A system that detects and identifies cable and seabed movement (tasks 2, 3) requires an architecture different from YOLO, since such tasks introduce a temporal aspect to the detection problem that is unlikely to be captured in a single image. Instead, machine-learning methods that are typically applied to video classification may be utilized to detect the movement in SAS imagery. Such methods are designed to learn spatiotemporal patterns and their mapping to the desired outcomes. YOLO architecture may be

expanded to incorporate three-dimensional processing (image length and width, time) and combined with Long Short-Term Memory (LSTM) methods for “remembering” images occurring early in a sequence. Data augmentation methods that apply random distortions to SAS imagery can be employed to realize a large enough dataset to train-test the advanced architecture, if necessary.

In addition to training our ATR algorithm on the cable fidelity problem, ThayerMahan is currently investigating the transition of the bounding box annotations to a more pixel-perfect, polygonal mask representation autonomously via a technique called instance segmentation. Reducing the amount of noise (in the form of background) that exists in bounding box annotations will result in a more defined annotation associated with the objects of interest and will enable the creation of more information-rich contact reports on the data we collect.

The current approach to the instance segmentation problem is two-fold. As referenced previously, to manually annotate a corpus of images for the task of ATR requires a non-trivial amount of time and human resources. While already expending mass amounts of time, effort, and funds to curate the SAS imagery via bounding boxes, the next step would be to find a weakly supervised algorithm that can translate the bounding box annotations into pixel-perfect instance segmentation masks. After which, the next step would be to find an algorithm to conduct the supervised instance segmentation itself.

4 Discussion

The results of the survey and system engineering analysis have demonstrated the advantages of SAS in the visualization and characterization of seabed infrastructure, cables, and environments. When considering the ACR and the ability to quickly acquire high resolution data independent of range and frequency, the SAS system’s benefits are quickly realized compared to traditional side scan sonars.

When looking at the commercial impact of SAS, a simple metric would be to look at it as a replacement for side scan systems. Side-scan surveys represent a sizable percentage of a wind farm’s life cycle and BOP maintenance practices. In proactive maintenance alone, side-scan is representative of about 0.94% of a wind farm’s Levelized Cost of Energy (LCOE) and the application of SAS could reduce that to 0.35% from the total in survey time efficiency alone. The lasting effects are substantial as well, although not quite as quantifiable. The benefit of a faster survey means that work can be completed in smaller windows which is significant considering degree of weather induced downtime with offshore surveys. Along with speed, the higher resolution allows for rapid and more accurate detection of damage (infrastructure, cable, etc.). Being able to quickly identify potential failures expedites the repair process and can ultimately reduce downtime of the system.

In order to validate the use of the system for damage analysis, the survey outlined in this report used emplaced targets to simulate damaged cables. The findings indicate that the SAS system is capable of identifying cables and the ATR program tests on this dataset illustrate that the overall system is capable of delineating damaged versus undamaged cable. This is difficult to reproduce with current SSS and MBES methodologies. A visual ROV survey is generally required to ascertain damage to cables on the seabed which is generally a longer and costlier endeavor.

4.1 Summary of Current Methodologies

Marine systems for underwater surveying will vary greatly depending on the operational need and the project requirements. Every type of system has its own limitations and benefits, and in many instances, a combination of platforms might be used to fulfill a project’s goal. Both towed systems (SeaScout) and vessel-mounted systems (R2Sonic) have been described in this report. Although each installation is different, both cases exemplify the physical benefits and issues inherent of such a system. Traditional survey platforms consist of towed systems, ROV’s, autonomous underwater vehicles (AUV), and vessel-mounted sensors with survey acquisition generally undertaken on multiple vessels and platforms. These include:

- An offshore vessel, for acquisition in water depths greater than 15-20m. This vessel often collects data with a hull mounted MBES, towed SSS and magnetometer systems, and hull mounted or towed sub-bottom profiler (SBP). ROV systems are sometimes used for visual inspection works on offshore vessels.
- An inshore vessel, for acquisition in water depths <15-20m to as far inshore as possible. This vessel acquires data typically with an over the side or hull mounted MBES, towed SSS and magnetometer systems and hull mounted or towed SBP.
- Autonomous Surface Vehicles (ASV), for acquisition in shallow water depths where vessels cannot operate. These vehicles generally acquire high resolution MBES data and are used to fill the data gap between onshore and marine surveys.
- Diver Surveys – these were traditionally used for the same shallow water environments but are now more commonly replaced with AUV and ROV technology.
- Drones or traditional land survey techniques for the onshore survey of cables. This involves acquisition of high resolution lidar data and photogrammetry data. Drones can be used to acquire the data gap also, depending on how far the inshore vessel can get to shore.

Two of the most prominent platforms that have yet to be discussed in this report are ROV's and AUV's. ROV's and AUV's aid in offshore wind surveying by visually following cables laid on the seafloor or through sensors designed to detect submerged objects. They are useful for surveying areas that are inaccessible by vessel, or towed platforms. Depending on project specifications they can be equipped with a series of sensors or survey equipment including cable trackers, MBES, SSS, laser sensors, and SBP. Both AUV's and ROV's are typically used in follow-up surveys as well if significant sediment scour, or hazardous conditions are identified prior. They each provide their own advantages and disadvantages with these surveys. For example, AUV's can make deep water turns faster, but they do not enable real-time data transfer and dynamic re-tasking. ROV's can be outfitted with a variety of sensors to enhance their capabilities but their simplest designs are equipped with cameras. Data collected is instantly transmitted via the ROV's tether to the topside operator.

AUV's on the other hand, can function underwater without constant input from an operator. They are programmed prior to survey on where, when, and what to do. AUV's are commonly outfitted with a variety of sensors to collect data, but unlike ROV's their data is stored in onboard computers and cannot be accessed until post operation. Similar to ROV's, they also vary in size, ranging from a few hundred pounds to increasing sizes of multiple tons. AUV's must be charged regularly to obtain the highest functionality as their propulsion and sensor payloads generally consume significant power. Their battery

life varies depending on the model but some AUV's have endurance of several days in larger systems. Ultimately, endurance is a function of the survey requirements and associated payload(s).

As mentioned previously, different payloads can be incorporated into different platforms to complete a survey. Most sensors are utilized for a specific task so multiple sensors can be used on the same platform to maximize the capabilities of the survey system. Current survey techniques of cables and wind farms generally comprise MBES, SSS, magnetometer and SBP systems. Areas with the potential for unexploded ordnance (UXO) are surveyed in accordance with a UXO specification designed to detect the minimum object threat assessed for the area. This is a specialist survey, not comparable with this SAS acquisition undertaken on this survey trial and therefore not detailed in this report.

4.2 Limitations of Marine Surveying Technologies

As indicated above, one of the limitations for towed SAS surveys is water depth. Survey acquisition on vessels is limited by the physical constraints of the bathymetry of the nearshore environment. Vessels can safely maneuver in water depths 2-3m deeper than the draft of the boat, including any sensors which may be hull mounted. This is however dependent on the vessel master and the other environmental factors of the landing area. As a result, there is generally a data gap between the inshore extents of the vessel and the inshore survey acquisition target. The same constraints however apply for traditional SSS survey acquisition, where this gap is generally filled with data acquired with an ASV, drone or diver survey. The same techniques could therefore be used for SAS survey acquisition.

Along with depth limitations, all marine systems have physical limitations as well. Due to the nature of subsea environments, all acoustic systems are subject to sound speed velocity fluctuations. This can be drastically seen in thermoclines, or areas of large thermal gradients. This can cause artifacts to be produced within the data which renders the imagery unusable. With real-time feedback platforms this is easily resolved by changing the system's altitude off the seafloor and getting the acoustic sensors below the thermal gradient. Hull-mounted sensors and AUV's, on the other hand, cannot easily correct for this on the fly and will generally require re-surveying the area with different optimized settings. Other environmental influences can also prove to be physical limitations Dense areas of sea kelp, for example, may inhibit cable detection with SAS however, in a similar fashion, kelp forests would also interfere with traditional SSS techniques. The SAS, due to its resolution, may however be able to be image the kelp itself, aiding benthic analysis of survey areas.

Other physical limitations, more specifically with side scan sonars, include the array length and depression angle. Due to the physics of sonar, the ability to beamform an acoustic signal is dependent on multiple factors such as speed, altitude, and array length. To make a simplification, the along-track resolution of a side-scan sonar system is generally limited by the length of the sonar array such that, in order to have a greater resolution at the same frequency, a longer sonar array would be required. Unlike traditional SSS, SAS achieves higher resolution by synthetically lengthening the array instead of physically. Due to the way the individual pings are stacked and beamformed, SAS systems can achieve higher resolution and longer range than side-scan sonars of the same size array. The other benefit is that the SAS systems are also frequency and range independent, whereas SSS would require varying frequency for various ranges to a target.

Existing marine systems all have their own specific requirements with respect to vessel, support equipment, operators, and logistics. These requirements, in one way or another, factor into the total cost of the survey and how the project goals are achieved. Geophysical and/or inspection surveys are generally undertaken in accordance with the client requirements. These vary on a project-by-project basis, depending on the overall aims of the survey. The SAS system is suitable for a wide range of projects, and as indicated in Section 3.5.3 above, initial findings indicate it has the ability to detect cable damage. Currently, visual inspection surveys are generally undertaken with MBES and ROV camera footage, however this ROV imagery is dependent on the water clarity and currents in the project area, as well as water depth. ROV survey acquisition is also much slower (~0.5 kt) than SAS acquisition and the ROV has a small visual window therefore it has to search for cables which are off the reported alignment. SAS has a much wider swath and therefore can cover more of the seabed in a shorter period of time.

In summary, there are operational limitations to the SAS as there are with traditional SSS techniques, however SAS can operate at survey speeds of 6-8 kts, therefore covering more seabed than traditional SSS which typically require survey speeds of 4 kts. Weather and sea state restrictions on launch and recovery of the SAS are similar to that of SSS, however the limit for SAS acquisition is around sea state 6, whereas standard geophysical acquisition with SSS and MBES is nearer sea state 3-4. SAS can also provide higher resolution imagery than traditional SSS and therefore can provide more details about the local activity, cable protection, obstructions and trends that may occur within a wind farm development.

In comparison to ROV's, the SAS swath width is much larger than the visual field of view obtained with ROV footage. With the ability to identify potential areas of cable damage in shorter timescales, SAS could prove to be a useful tool for monitoring surveys on wind farm and cable route developments. It is envisaged that the system could be used in conjunction with ROV systems within these routine monitoring surveys – data could be acquired with SAS, with ROV imagery used to target areas of concern as required. This tandem survey would allow for rapid detection and target interrogation.

Another limitation of current surveying systems is their ability to detail the biological habitat of the environment. Most biological mapping would require visual inspection by ROV which is a slow and laborious process. SAS technology could be utilized for benthic/environmental surveys as it will provide higher resolution data than traditional SSS data, therefore more likely to identify changing textures in the seabed which can indicate benthic habitats. This could, in turn, reduce the time to perform biological surveys, and when used in tandem with ROV's, a SAS survey can decrease the amount of camera time required for visual inspection. Prior SAS projects have acquired data over 3–4-inch cables surface laid over coral reef and imaged the cables clearly. As well the SeaScout System has been used in mapping benthic and mussel habitats of the Long Island Sound.

4.3 Key Findings

The results of this survey have demonstrated the multiple facets, in which, SAS surveys could be implemented in the wind farm industry to improve upon existing survey methodologies. The findings have validated the rapid coverage rate of the system and the utility of high-resolution imagery in assessment of infrastructure and the seabed.

By utilizing historical imagery and gathering simultaneous data from secondary survey sensors (multibeam), a direct comparison could be made to the SAS imagery. In terms of resolution, the benefits of the SAS are obvious relative to the secondary multibeam sensors. Being able to collect range and frequency independent data, the SAS payload allows for elucidation of small-scale targets (such as cables) in wide swaths. This degree of granularity also allows for the detection of minute changes in the seabed environment. With repetitive surveys at a site, the SAS allows for a detailed temporal comparison of the area as well.

With regards to cable surveying and detection, the SeaScout system was not only able to detect the presence of cables, but also detail whether they were damaged and inform on their severity. The ability to

analyze this in real-time, with the rapid coverage rate of the system, allows for immediate feedback and can drastically cut down on mitigation response times and potential down time. Also, being able to understand the severity of the damage from the SAS imagery can also better inform the response measures taken without the use of additional survey methods.

This study also looked at the improvement upon data processing with SAS in regard to target recognition and machine learning. The data produced by the SAS is significant, generating approximately 300 GB/hr. With this amount of data, a labor-intensive processing endeavor is undergone in order to identify and characterize targets. The use of AI in ATR looks to reduce this processing time and produce high confidence results. As discussed in the previous sections, this utility is rapidly evolving and with larger surveys and greater datasets it is becoming more valuable.

4.4 Relevancy and Market Impact

As mentioned earlier, the application of SAS in the commercial space has significant savings potential in the offshore wind market. Not solely with respect to its efficiency, but also in application for preventative measures. To put the potential savings into perspective it is best to equate the savings to the LCOE of a wind farm, as to have a tangible metric. The following analysis breaks down the impact SAS could have on LCOE with respect to time savings and potential damage prevention.

It is estimated that the overall capital expenditure of surveys attributed to the LCOE is around 0.83% per installed megawatt (MW), based upon a 105 MW wind farm with fifteen 15 MW turbines (Alsubal et al. 2021). As mentioned earlier, one of the greatest advantages of SAS implementation is the rate at which high resolution data can be collected. With an ACR approximately six times faster than traditional sonar methods, the costs for performing a survey are reduced by about 85% (excluding planning and processing costs). Assuming the operational survey time represents about half of the overall survey expenditures, from the estimated hydrographic survey costs, the potential savings can be seen at \$12,477/MW ($\$30,066 * 0.5 * 0.85$). This reduction in capital expenditure will translate directly to LCOE and will represent an overall estimated 0.35% decrease in the total wind farm. Note, estimated survey costs discussed in the above reference.

There are additional benefits when considering the operational expenditure savings. Proactive maintenance alone is estimated to comprise 5.22% of total LCOE. Within proactive maintenance, surveys represent approximately 18% (half of Balance of Plant (BOP) services over the total maintenance and

service costs per BVG Associates 2019) which is 0.94% of total LCOE. Considering the same time savings estimation as above, the impact of SAS on proactive maintenance is a 0.4% savings.

Aside from survey speed, there is additional impact in the utility of SAS by way of minimizing corrective maintenance and insurance costs. Those two factors represent an additional 6.87% of total LCOE. Large scale corrective maintenance procedures can cost up to \$7 million USD, and corrective maintenance attributed to cable failure comprise 75-80% of overall insurance claims (Dinmohammadi et al. 2019). The severity of these failures can be directly mitigated with more effective preventative maintenance such as the implementation of SAS. As mentioned previously, a single inter-array cable failure repair costs approximately \$7 million United States Dollar (USD) while failure of an export cable can range from \$16 to \$20 million USD. Being able to prevent one inter-array failure event ($\$7,000,000 / (\$160,550 \text{ per MW} * 105 \text{ MW})$) represents a 41.5% percent savings of corrective maintenance costs with a total LCOE reduction of 1.85% over the life cycle of a wind farm. Taking all potential savings into consideration, SAS has the potential to save 2.6% on the total lifetime LCOE. This savings strengthens with scale and will only grow larger with greater industry acceptance. The reader should note that these representative figures are derived from NYSERDA Deliverable 1.2.1 NYSERDA Contract 115 February 2022 from a specific wind farm and may be different based on time of installation, geographic location, and overall size. Assumptions have been made to illustrate potential savings via enhanced survey procedures for generalized purposes. (NYSERDA, *Levelized Cost of Energy Market Impact Analysis: Alternative Survey Methods*, Agreement 115. Prepared by, ThayerMahan Inc.).

The evolution of SAS in the commercial market is dependent on multiple factors. The first is the limited availability of these systems and their acceptance as a suitable sensor for commercial use. Prior research and commercial work have demonstrated the capabilities of SAS and its abilities to meet International Hydrographic Organization standards and customer specifications. As SAS projects continue to grow, the commercial demand will also increase. As seen in existing Request for Proposals, this is just starting to take place. Another roadblock for the commercialization of SAS is with respect to the output data. The TIL format is a proprietary format and has only been implemented in a couple commercial hydrographic software packages which limits the ability to post-process and work with the data, in a usable, hydrographic sense. To make the system more attractive to the widespread industry, implementation of the TIL file type in more hydrographic software would help catalyze commercialization.

4.5 Future Work

The sea trials undertaken have proven the high-quality data resolution of the SAS system, and this report details the potential cost savings utilizing the system can achieve. The trials were however limited by budgetary constraints and the length of cable available for survey. Simulated targets used were limited to five, 3m lengths of 33Kv inter-array power cable and therefore any assessment of the SAS capabilities is limited to what could be achieved with such lengths of cable. Future work would involve multiple survey passes over larger sections of cable, and the use of additional targets to simulate typical cable exposures. Varying degrees of damage would be applied to this cable to mimic natural abrasion and third-party damage from fishing and anchors. Longer sections of cable would also allow the potential to assess for damage in crowning cables, as well as exposed and spanning sections.

The integration of SAS data into standard software packages for post process analysis should also be considered. Files are currently exported as .TIL files and there is limited commercial software which can use these however the simultaneous export of GeoTiff files are therefore supported by most GIS software, allowing the mosaics to be used for post processing evaluation.

Finally, future projects could assess the cost savings of cable repair ahead of failure. As detailed in Section 4.4 above, prevention of 1 IAC failure represents a 41.5% saving on corrective maintenance costs with total LCOE reduction of 1.85% over life cycle of wind farm.

Typical geophysical surveys on wind farms and cables generally utilize SSS and MBES along with other sensors such as magnetometer and sub bottom profilers etc., depending on the project requirements. Visual inspections are currently undertaken with ROV and MBES systems. An analysis of the following typical costs is recommended to understand how the SAS could influence project budgets over the lifetime of a wind farm:

1. SAS survey compared with SSS and MBES survey of similar scope for general wind farm inspection survey.
2. SAS survey compared to ROV and MBES for scope requiring visual inspection works.
3. SAS survey, with ROV video footage over targeted areas of interest for visual inspection works.

The costs for scenario 3 will provide an assessment of costings for proactive, rather than reactive, cable management. Proactive management may include regular monitoring undertaken with the SAS, with periodic ROV visual inspection work for targeted areas of concern. This would allow the wind farm operator to identify areas where additional cable protection may be required and, in extreme cases, the installation of redundancy cables to ensure continued power generation in cases where there is a high risk of cable failure. Reactive cable management would imply a scenario where a cable fails, a visual survey undertaken, and the cable replaced with some associated down time on one or more turbines in the array.

Proactive cable management could also look at the locations in which SAS would be most beneficial. High resolution data, acquired over a shorter survey period, would be highly beneficial in areas where the seabed is mobile, with an increased risk of scour and seabed movement causing cable exposures; or areas where the current is significant and can cause abrasion on areas of surface laid cable etc. SAS could be used in conjunction with traditional SSS surveys and limited to areas around turbine bases, cable/scour protection etc. in wind farm developments where the risk of cable exposure is less significant, or the seabed is not considered to be mobile.

5 Conclusions

In support of project aims, this document highlighted the potential causes for cable failure and the potential impact of mitigation with preventative maintenance Synthetic Aperture Sonar (SAS) surveys. Along with cable failure, being the focus of this study, the SAS system also demonstrated possible applications throughout commercial offshore wind development. In order to maximize the production from offshore wind it is imperative to regularly maintain infrastructure and cables, as to minimize downtime and prevent unplanned outages. Utilization of rapid, high-resolution, routine SAS surveys has the potential to greatly facilitate these maintenance operations and create significant long-term cost savings for developers and taxpayers.

The demonstration survey successfully completed its three main goals: (1) to identify and map existing cable infrastructure, (2) to demonstrate short-term, small-scale changes in bathymetry, and (3) create a representative database of SAS imagery to simulate exposed cable sections. In support of these goals the system accomplished the four supporting sonar evaluation tasks by:

- (1) Detecting evidence of fishing gear in the vicinity of cables.
 - a. In Figure 11, this is most easily seen with the presence of ghost fishing gear. Also, along the survey corridor there were fish trawling as defined by the equally spaced drag marks along the seabed.
- (2) Detecting cable movement
 - a. This can be seen in the simulated target E where the cable was warped to simulate an anchor drag, as well as in Figure 16 where the effects of line drags can be evidenced throughout the seabed and in the fishing gear.
- (3) Detecting seabed movement
 - a. The presence of the dynamic seabed environment was shown throughout the survey, especially in areas of sand waves. These areas showed how the sediment can shift and how burial and scour effects could be present in subsea infrastructure.
- (4) Detecting cable damage where exposed.
 - a. This was tested and verified by the results of the simulated target survey. By imaging targets of varying damage and comparing their imagery and intensities, it was possible to elucidate the degree of damage of the cable and where they were emplaced.

These tasks and goals were achieved in two at-sea main survey events. One being the survey of the BIWF cable corridor and infrastructure, and the second being the surveying of simulated damaged cables. The data collected by both surveys successfully demonstrated the applicability of SAS to the offshore wind

market and how adaptation of such a system can provide a degree of insight and efficiency that has yet to be seen with existing commercial systems. The SeaScout SAS system could be a beneficial tool to offshore survey and one that would be complementary to current and widespread survey technologies.

6 References

- Alsubal, Shamsan, Wesam Salah Alaloul, Muhammad Ali Musarat, Eu Lim Shawn, M. S. Liew, and Pavitirakumar Palaniappan. 2021. "Life Cycle Cost Assessment of Offshore Wind Farm: Kudat Malaysia Case." *Sustainability (Switzerland)* 13 (14). doi:10.3390/su13147943.
- Dinmohammadi, Fateme, David Flynn, Chris Bailey, Michael Pecht, Chunyan Yin, Pushpa Rajaguru, and Valentin Robu. 2019. "Predicting Damage and Life Expectancy of Subsea Power Cables in Offshore Renewable Energy Applications." *IEEE Access* 7. IEEE: 54658–69. doi:10.1109/ACCESS.2019.2911260.

Appendix A: Calibration and Engineering Analysis

Dimensional Control Survey

An on-water dimensional control survey was performed by a qualified third party-surveyor between April 19th and 20th, 2022. The survey was performed at the dock while the vessel was in water using a laser total station. A centerline was established along the fore-aft (Y) axis of the vessel. The shots were collected relative to a plane established using multiple deck shots. The origin of the survey was set as a point at the stern on the centerline and was shifted to the RP during processing. The vessel RP was on the vessel centerline in line with the POSMV IMU.

The survey pole was shot-in while horizontal and then common points were shot with the pole deployed in a vertical position. The pole reference points were then aligned to the vessel reference frame. A table of the relevant shots is provided below. The table includes the specific sensor offsets and elevations relative to both the vessel RP and waterline.

Figure A- 1. USBL Pole.

DCR target positions on the USBL pole for measuring the system offsets.

(ThayerMahan, Inc.)



Table A- 1. DCR Results.

DCR target positions on the USBL pole for measuring the system offsets.

(ThayerMahan, Inc.)

Shot Description	DCR Shots			Device Offsets			Device Coordinates w.r.t. RP			Device Notes	Device Coordinates w.r.t. waterline		
	X [+ Stbd]	Y [+ Fwd]	Z [+ up]	X [+ Stbd]	Y [+ Fwd]	Z [+ up]	X [+ Stbd]	Y [+ Fwd]	Z [+ up]		X [+ Stbd]	Y [+ Fwd]	Z [+ up above waterline]
RP	0.000	0.000	0.000	0.000	0.000	0.000	0.000	0.000	0.000	No device associated	0.000	0.000	0.958
POS MV IMU Plate Center	-2.062	0.000	0.331	0.000	0.000	0.105	-2.062	0.000	0.436	Point offset to top of IMU	-2.062	0.000	1.394
Accom. Container - Port-aft, top of threaded rod Primary POSMV antenna	-5.654	0.610	3.607	0.000	0.000	0.039	-5.654	0.610	3.646	Offset to antenna phase center	-5.654	0.610	4.603
Accom. Container - Port-aft-inset, top of threaded rod Primary VS1000 antenna	-4.375	0.556	3.621	0.000	0.000	0.026	-4.375	0.556	3.647	Offset to antenna phase center	-4.375	0.556	4.604
Accom. Container - Stbd-aft-inset, top of threaded rod Secondary VS1000 antenna	-3.203	0.552	3.629	0.000	0.000	0.026	-3.203	0.552	3.655	Offset to antenna phase center	-3.203	0.552	4.612
Accom. Container - Port-aft, top of threaded rod Secondary POSMV antenna	-1.943	0.596	3.612	0.000	0.000	0.039	-1.943	0.596	3.651	Offset to antenna phase center	-1.943	0.596	4.608
Office Container - port-aft, top of threaded rod Tertiary GNSS	2.049	-4.134	3.422	0.000	0.000	0.029	2.049	-4.134	3.451	Offset to antenna phase center	2.049	-4.134	4.409
Office Container - stbd-aft	5.522	-4.146	3.446	0.000	0.000	0.000	5.522	-4.146	3.446	Not being used	5.522	-4.146	4.404
MBES Flange (forward) punch	-6.944	-0.665	-5.142	0.000	0.000	0.000	-6.944	-0.665	-5.142	Not being used	-6.944	-0.665	-4.185
MBES Flange Face Center	-6.936	-0.777	-5.154	0.000	0.182	-0.321	-6.936	-0.595	-5.472	Offset to acoustic center	-6.936	-0.777	-4.515
USBL Flange (aft) punch	-6.885	-1.454	-5.274	0.000	0.000	0.000	-6.885	-1.454	-5.274	Not being used	-6.885	-1.454	-4.317
USBL Flange Face Center	-6.870	-1.593	-5.287	0.000	0.000	-0.019	-6.870	-1.593	-5.306	Offset to GAPS reference point	-6.870	-1.593	-4.349
Pole 'T' aft top threaded rod	-6.758	-1.932	2.805	0.000	0.000	0.000	-6.758	-1.932	2.805	Not being used	-6.758	-1.932	3.763
Pole 'T' middle top threaded rod	-6.827	-1.104	2.795	0.000	0.000	0.000	-6.827	-1.104	2.795	Not being used	-6.827	-1.104	3.753
Pole 'T' forward top threaded rod	-6.896	-0.275	2.776	0.000	0.000	0.000	-6.896	-0.275	2.776	Not being used	-6.896	-0.275	3.734
Measure Down - Port	-6.698	-1.725	-0.007	0.000	0.000	0.000	-6.698	-1.725	-0.007	No device associated	-6.698	-1.725	0.951
Measure Down - Stbd	6.691	-3.936	0.004	0.000	0.000	0.000	6.691	-3.936	0.004	No device associated	6.691	-3.936	0.962
Centerline - Aft	0.000	-21.271	0.000	0.000	0.000	0.000	0.000	-21.271	0.000	Not being used	0.000	-21.271	0.958
Centerline - Forward	0.000	7.596	-0.010	0.000	0.000	0.000	0.000	7.596	-0.010	Not being used	0.000	7.596	0.948

MRU Alignment

The MRU misalignment angles were calculated based on the dimensional control survey MRU/IMU plate extension shots that were collected on April 19th and 20th, 2022. The yaw/heading misalignment result is an average of the yaw misalignments calculations in both the X and Y axes. The resulting angles are as follows along with photos of the IMU placement on the deck:

Roll: 0.099 deg (the port side of the IMU plate is above the starboard side)

Pitch: 0.198 deg (the bow side of the plate is above the stern side)

Yaw/Heading: -0.222 deg (the plate is rotated counterclockwise if viewing from above)

Figure A- 2. MRU.

Image of MRU alignment and positioning on the vessel.

(ThayerMahan, Inc.)



Survey Equipment

The following table lists the major survey equipment systems, outside of the SeaScout system, mobilized for this survey. A generalized equipment interface diagram is shown early in this document. Calibration sheets for the sound speed sensors are provided later in the Appendix.

Table A- 2. Equipment.

Survey equipment, models and serial numbers are listed within the table.

(ThayerMahan, Inc.)

System	Manufacturer	Model	Serial Number(s)
Vessel INS	Applanix	POSMV Oceanmaster	12701/5706
<i>Vessel INS - Antennas x 2</i>	Trimble	540AP	
Secondary GNSS	Hemisphere	VS1000	19505340
<i>Secondary GNSS - Antennas x 2</i>	Hemisphere	A45	
USBL	GAPS	G4 (M7)	282
USBL – Beacon	iXBlue	MT912S	843
MBES	R2Sonic	2024	101934 (head) 104646 (sim)
<i>MBES - Sound Speed</i>	Valeport	miniSVS	80693
Sound Speed Profiler	AML	AML-3 LGR	A30520
SV	AML	SV.X2	210606
<i>Pressure</i>	AML	P.X2	308221
<i>Pressure</i>	AML	P.X2	307342

Dockside Calibrations and Verifications

Shore Control Checks

The published OPUS shared solution: benchmark 9050 C 2014 (PID: BBDM39) was checked to using a rover GNSS on April 18th, 2022. A copy of the recovery sheet is provided in the Appendix. The position was checked using both NYSNET (New York State Spatial Reference Network) [NAD83(2011)] and Atlas H10 (ITRF08) correctors. The Atlas corrected positions were transformed in real time using HYPACK’s 7-parameter transformation and the 2018 Geoid model. These checks were performed in NAD83(2011) UTM 18N and NAVD88 elevations.

Figure A- 3. Benchmark 9050 C 2014.

Image of GNSS setup for position verification test.

(ThayerMahan, Inc.)



Table A- 3. Position Control Checks.

Positional control tests and results from established point.

(ThayerMahan, Inc.)

Name	UTM18 coordinates (NAD83) 2010.0		
	Easting	Northing	Ortho Height (m)
851 9050 C	579,424.65	4,496,190.07	11.801

Date	Time		Benchmark	Check Coordinates			XY Delta (m)	Elevation Delta (m)	Comments
	UTC	Local		Easting (m)	Northing (m)	Elevation (m)			
4/18/2022	16:26	12:26	851 9050 C	579,424.63	4,496,190.10	11.826	0.04	0.03	RTK Average (NYSNet) nearest. No datum transformation. Correctors in NAD83(2011).
4/18/2022	18:43	14:43	851 9050 C	579,424.63	4,496,190.08	11.826	0.03	0.03	RTK Average (Atlas correctors). HTDP parameters 7-param transformation. Ortho corrector applied for z-transformation.

A TBM (temporary benchmark) ‘ML2022-01’ was set at a fixed bulkhead near the vessel. This point was established using a 4+ hour static observation that was submitted to the NGS Online Positioning User Service (OPUS). A copy of the report is provided in the Section 0 Appendix. The resultant coordinates were provided in NAD83(2011) and NAVD88 (vertical). A RTK position check was performed to this point using NYSNET NTRIP correctors to further confirm the position. The elevation of the point was adjusted to MLLW using VDATUM and a conversion value of 0.844m.

Figure A- 4. Temporary Benchmark.

Image of GNSS setup for establishing TBM.

(ThayerMahan, Inc.)



The following is a table of the established coordinate for ML2022-01. These coordinates are provided in UTM zones 18 and 19.

Table A- 4. TBM Position.

Positioning for the TBM.

(ThayerMahan, Inc.)

Name	UTM18N coordinates (NAD83 2011) (2010.0)		Ortho Height (m)	MLLW Elev. (m)	UTM19N coordinates (NAD83 2011) (2010.0)		Comments
	Easting (m)	Northing (m)			Easting (m)	Northing (m)	
ML2022-01	578,359.28	4,498,821.71	1.693	2.537	70,901.96	4,510,798.92	OPUS Results

GNSS Health Check and Position Comparison

Table A- 5. GNSS Health Check

Positioning verification of GNSS data

(ThayerMahan, Inc.)

Start Time (UTC):	2022/04/21 21:11:48	
End Time (UTC):	2022/04/21 22:10:15	
Duration (hh:mm:ss):	0:58:27	
Source File:	2022BM1112111_0.raw	
Data Rate Used for Analysis (hz):	1	
Average Coordinates (NAD83)	Easting (m)	Northing (m)
Primary GNSS/INS	70,937.35	4,510,795.55
Secondary GNSS	70,937.57	4,510,795.55
Correctors:		
Primary GNSS/INS:	Marinestar (WGS84/ITRF14 assumed ITRF08)	
Secondary GNSS:	Atlas H10 (WGS84/ITRF08)	
Primary position 95% confidence (+/-):	0.12	m
Secondary GNSS 95% confidence (+/-):	0.11	m
95% confidence difference (2-sigma) between primary and secondary positions:	0.08	m
Distance between average positions:	0.22	m

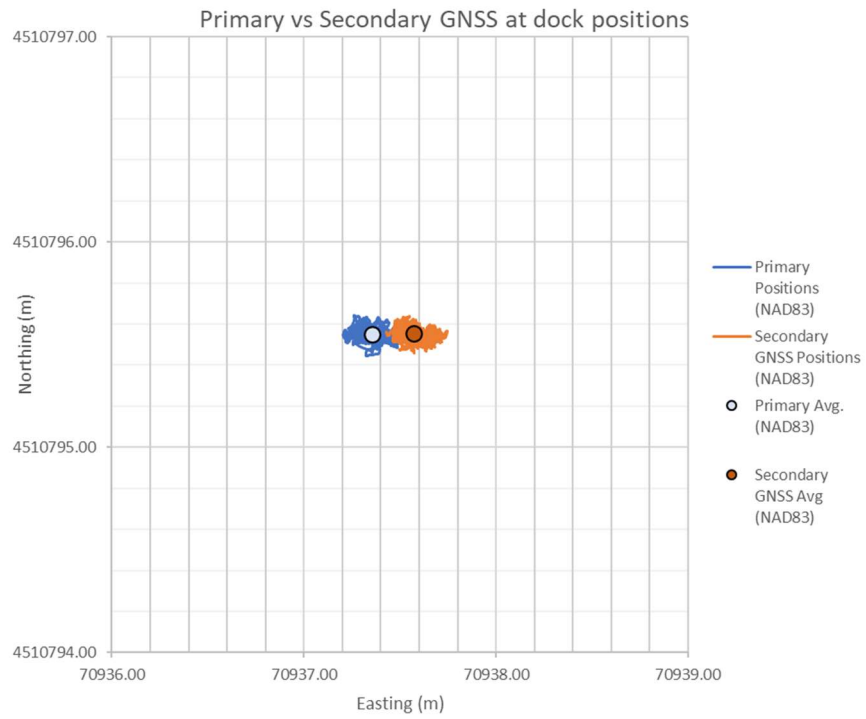
Note:

Data collected while vessel tied alongside floating dock.

Figure A- 5. GNSS Health Check Positioning.

Graph of GNSS positioning.

(ThayerMahan, Inc.)



Heading Health Check and verification

Table A- 6. Heading Health Check.

Heading verification of INS data.

(ThayerMahan, Inc.)

Heading Validation and Verification

Start Time (UTC):	2022/04/21 21:11:48
End Time (UTC):	2022/04/21 22:10:15
Duration (hh:mm:ss):	0:58:27
Source File(s):	Cal_2022BM11112111_0.raw
Data Rate Used for Analysis:	1 hz
Average Reported Heading:	82.46 deg
RTK vessel heading check avg.:	82.56 deg
INS vs RTK heading diff:	-0.10 deg
Average Calculated StdDev (10 seconds):	0.024 deg

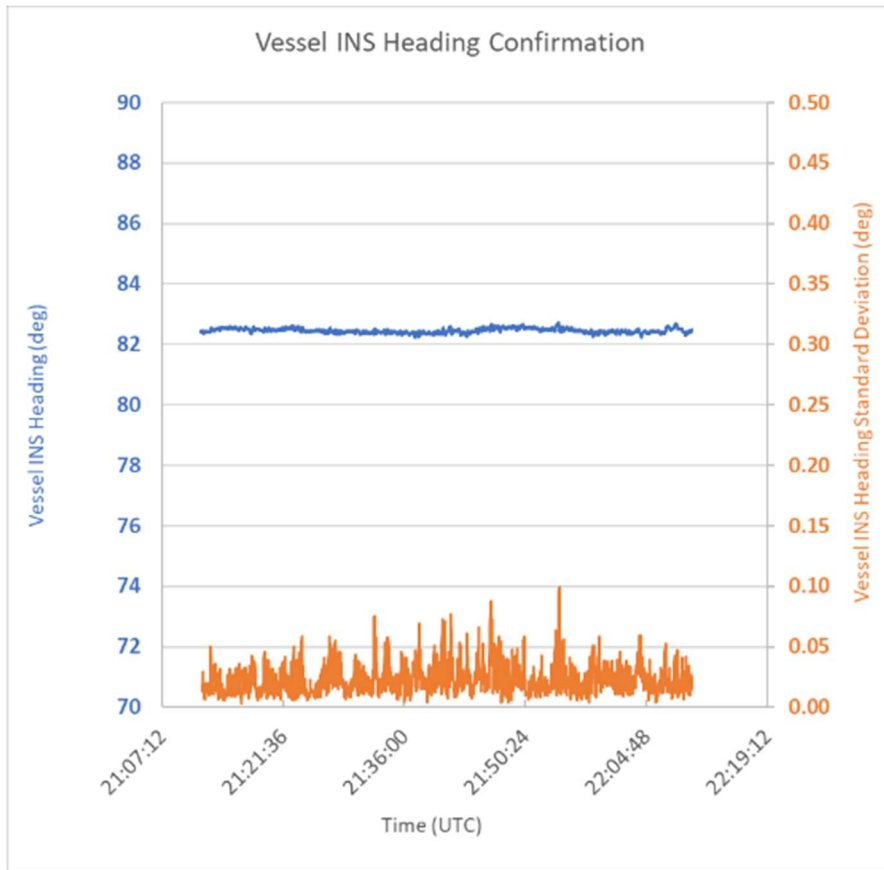
Notes:

-Calculated standard deviation based on 10sec rolling average.

Figure A- 6. Heading Health Check.

Graph of heading throughout duration of test.

(ThayerMahan, Inc.)



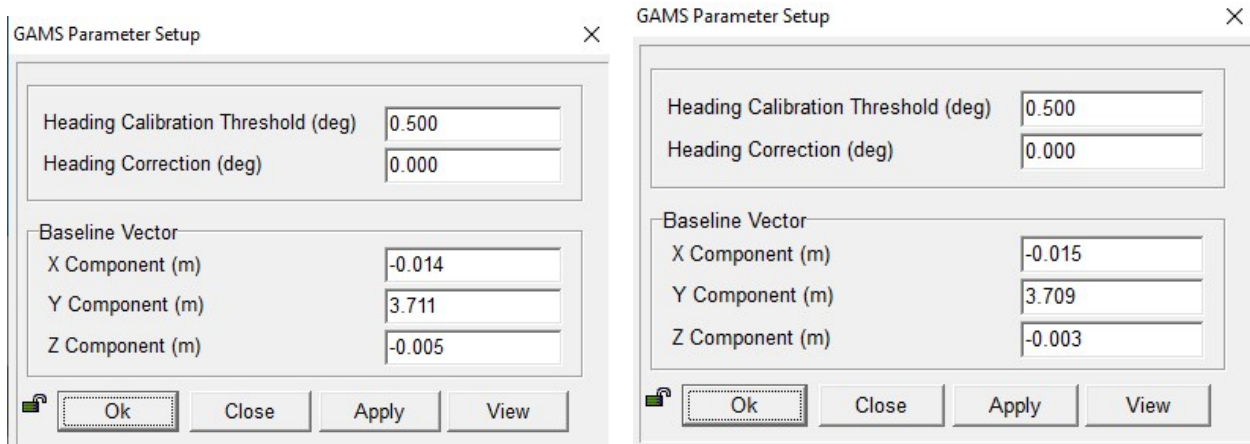
GAMS Verification

On April 23, 2022, a GAMS calibration was performed on the POSMV. The calibration values were compared to the ‘as-surveyed’ values from the DIMCON survey with favorable results. The as-surveyed values were used.

Figure A- 7. GAMS Verification.

(Left) As-surveyed GAMS parameter (used). (Right) GAMS calibration verification results.

(ThayerMahan, Inc.)



GNSS Tide Check and Vertical Transformation Verification

Measure downs were collected from the established TBM (ML2022-01) on April 21st (local).

Overlapping GNSS tide data were collected from the vessel while at dock during this time. A comparison of the real-time tides, the measured down water levels and preliminary water levels from the nearest NOAA tide gauge (The Battery, NY [8518750]) were compared in the datum of MLLW. The GNSS tides used in this comparison have not been filtered or smoothed. The results from this comparison are presented below:

Table A- 7. Vertical Tide Check.

Vertical tide check and GNSS comparison.

(ThayerMahan, Inc.)

Benchmark	Ortho Height (m)	MLLW Elev. (m)
ML2022-01	1.69	2.54

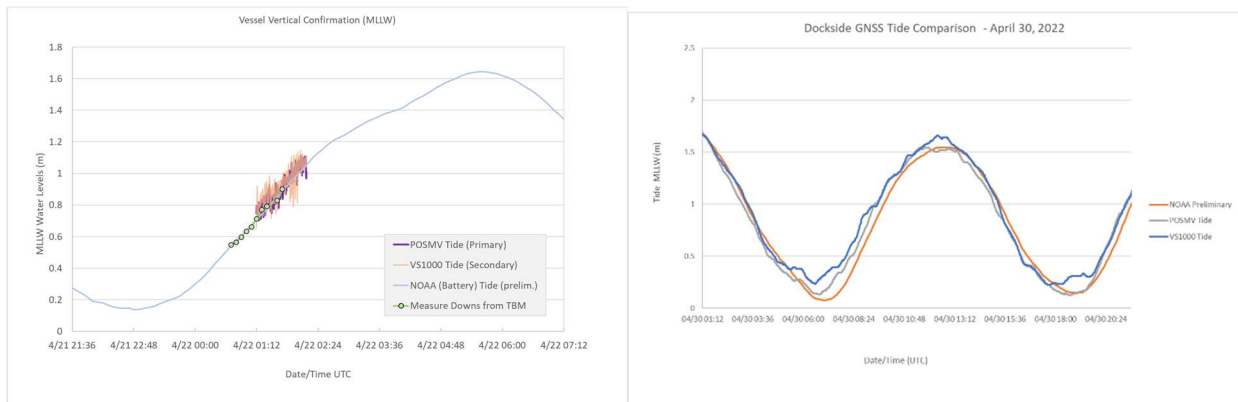
Date	Time (UTC)	Measure Down (m)	Water level Elevation NAVD88 (m)	Water Level Elevation MLLW (m)	POSMV Tide (MLLW) (m)	VS1000 Tide (MLLW) (m)	POSMV Tide Difference (m)	VS1000 Tide Difference (m)
22-Apr	01:12	1.82	-0.13	0.71	0.77	0.69	0.06	-0.02
22-Apr	01:18	1.77	-0.07	0.77	0.83	0.85	0.06	0.08
22-Apr	01:24	1.74	-0.05	0.79	0.86	0.92	0.07	0.13
22-Apr	01:36	1.71	-0.01	0.83	0.85	0.89	0.02	0.06
22-Apr	01:42	1.63	0.06	0.90	0.93	0.94	0.03	0.04

An additional dockside tide verification was performed using GNSS data collected while moored at dock. These data were thinned and smoothed using the workflow intended for the real-time data application. The GNSS data were again compared to the NOAA tide station at The Battery, NY and the comparison plot is provided below.

Figure A- 8. Vertical Transformation Verification.

(Left) Measured and reported tides. (Right) Vertical verification.

(ThayerMahan, Inc.)



On-Water Calibrations and Verifications

Bar and Spot Checks

Prior to the project commencing bar and spot checks were performed to confirm the draft of the MBES on April 27, 2022. The results from these checks are provided below.

Table A- 8. Bar Check.

Depth verification results.

(ThayerMahan, Inc.)

Date	27-Apr
Time (UTC):	12:13
Time (Local):	08:13
MBES Draft (m):	4.52

Bar Depth (m)	Recorded Depth (m)	Delta (m)
8.00	8.03	0.03
10.00	10.03	0.03
12.00	12.00	0.00
14.00	13.99	-0.01
16.00	16.07	0.07

Spot Depth (m)	Recorded Depth (m)	Delta (m)
17.38	17.41	0.03

Sound Speed Comparisons

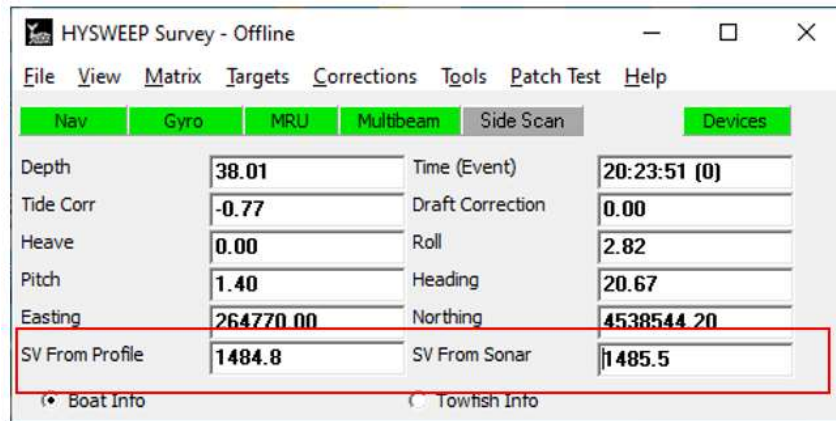
Profiler to MBES Surface Sensor

The cast data were loaded into Hysweep Survey and compared to the real-time sound speed reported at the MBES sensor. In the following example, these data compared to 0.7 m/s. This comparison can be made continuously during survey to monitor deviations from the previous sound speed profile. An alarm threshold, typically 2m/s, is set to notify survey when deviations are detected.

Figure A- 9. Sound Speed Comparison.

Profile reported and sonar reported sound velocity (In red box).

(ThayerMahan, Inc.)



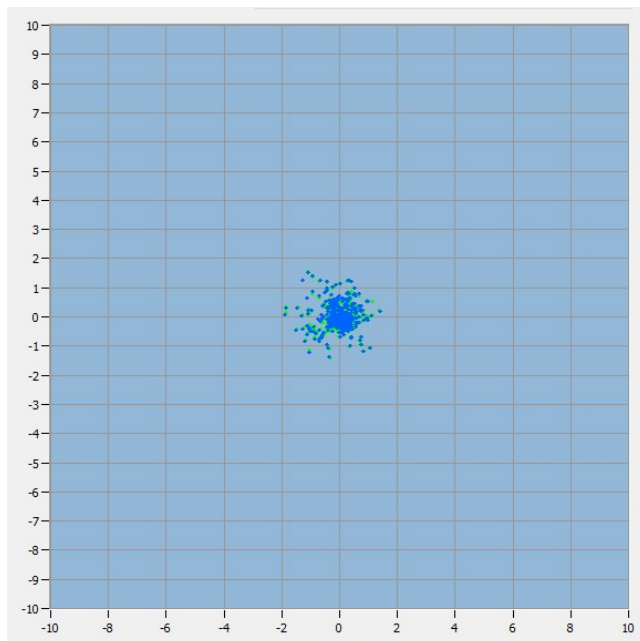
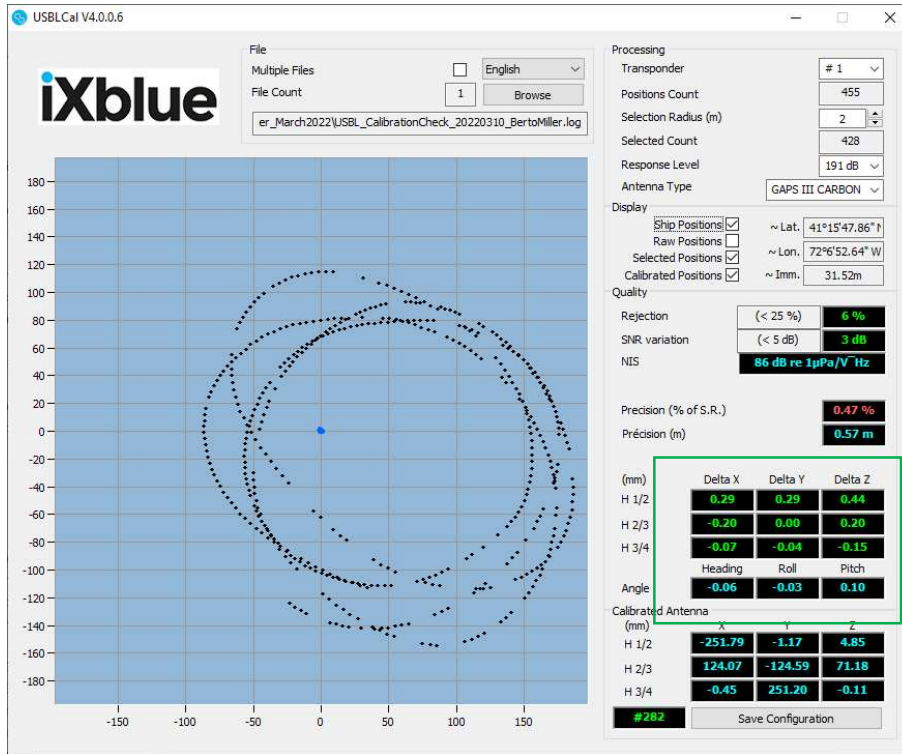
USBL Calibration

The primary GAPS USBL system (SN: 282) used for this survey was last calibrated on March 10, 2022, in Long Island Sound. Multiple circles were logged while navigating around a static beacon placed on the seafloor at nominal distances of approximately 50-190m in ~32m of water. The calibration involved an iterative process during which the calibration values were refined until the antenna (acoustic) residuals were within an acceptable range as shown in the below image with all 'green' values signifying acceptability. The calibration was processed using iXblue's USBLCal software.

Figure A- 10. USBL Calibration.

(Top) USBL Cal reported results (Deltas in green box). (Bottom) Point distribution of returns.

(ThayerMahan, Inc.)



MBES Patch Test

A patch test of the R2Sonic was performed to determine system angular offsets. The data were collected over distinct features. The patch test values were initially determined using Hypack, then confirmed in CARIS. The patch test comprised four tracklines that included two sets of reciprocal pairs offset approximately 40-meters from each other.

The following patch test values were determined:

Roll: 0.52 deg

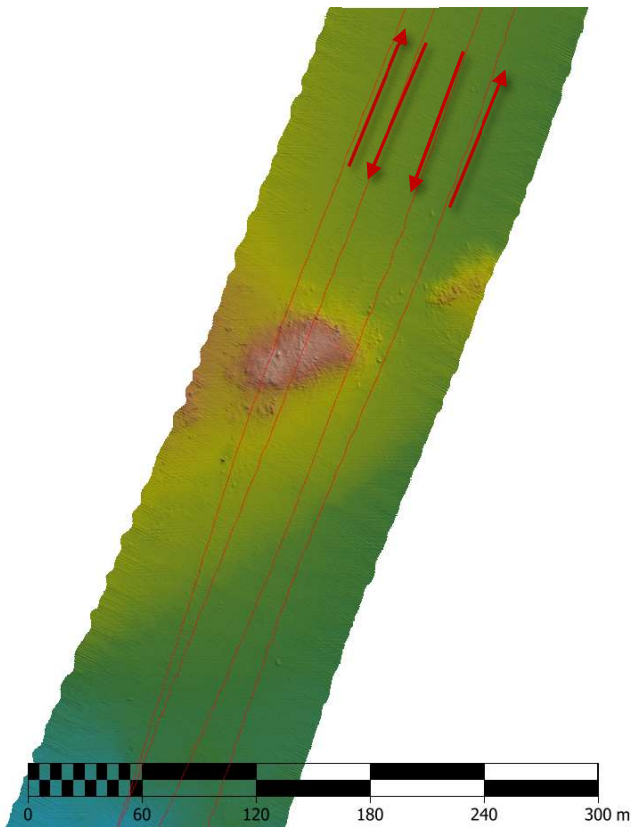
Pitch: -1.09 deg

Yaw: -1.15 deg

Figure A- 11. MBES Patch Test.

Representation of MBES patch test lines over the feature.

(ThayerMahan, Inc.)



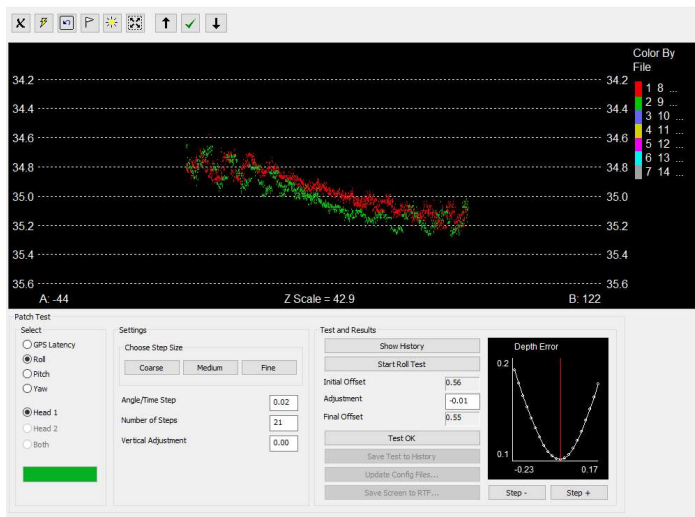
Roll

Reciprocal lines were compared (lines 1 and 2) over the relatively flat portions of the seafloor and compared to determine the system roll offset. Lines 3 and 4 provided a secondary set of comparison lines if needed.

Figure A- 12. Patch Test: Roll.

Graph of system roll and offset determination.

(ThayerMahan, Inc.)



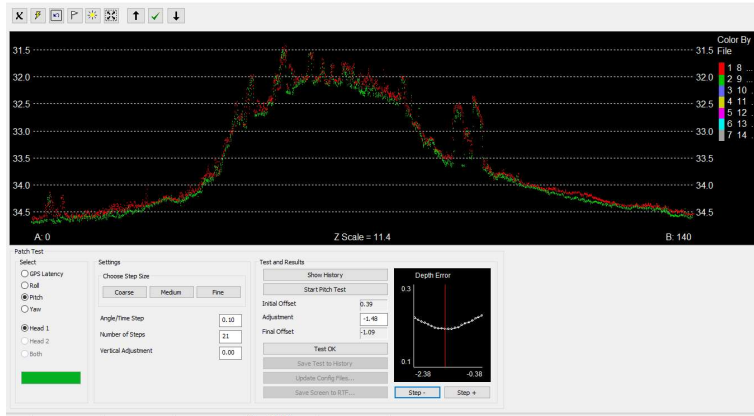
Pitch

Reciprocal lines were compared (lines 1 and 2) over the outcrop to determine the system pitch offset. Lines 3 and 4 provided a secondary set of comparison lines if needed.

Figure A- 13. Patch Test: Pitch.

Graph of system pitch and offset determination.

(ThayerMahan, Inc.)



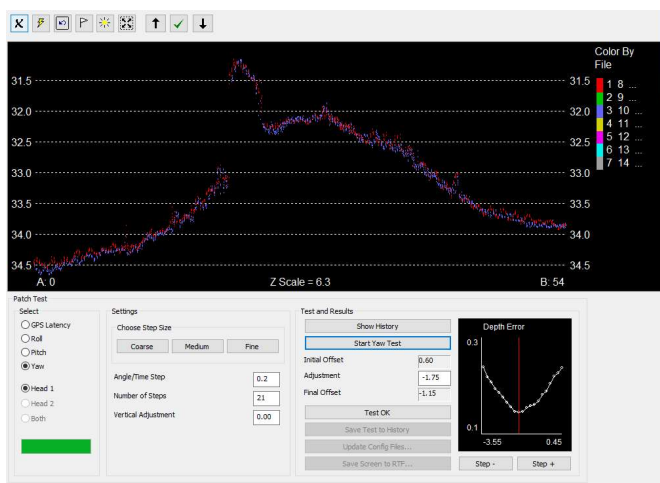
Yaw

Parallel and offset lines collected going the same direction were compared (lines 1 and 3) over the outcrop to determine the system yaw offset. Lines 2 and 4 provided a secondary set of comparison lines if needed.

Figure A- 14. Patch Test: Yaw.

Graph of system yaw and offset determination.

(ThayerMahan, Inc.)



Published Benchmark Datasheet

Shared Solution

PID: BBDM39
Designation: 851 9050 C
Stamping: 9050 C 2014
Stability: Monument will probably hold position well
Setting: Stainless steel rod in sleeve (10FT+ or 3.048M+)
Description: THE BENCH MARK IS SET IN THE GRASS NEAR THE EDGE OF THE BLUFF OVERLOOKING THE US COAST GUARD STATION BOAT BASIN, 57.50 M (188.6 FT) NORTH OF THE FLAGPOLE IN FRONT OF THE BRICK RESIDENCE, 12.48 M (40.9 FT) ESE OF THE GATE IN THE FENCE ALONG THE NORTH SIDE OF THE COAST GUARD STATION, 11.96 M (39.2 FT) NE OF AN UNUSED FLAGPOLE, 6.58 M (21.6 FT) NNW OF THE CONCRETE POST AT THE NE CORNER OF THE PICNIC SHELTER AND 1.85 M (6.1 FT) WEST OF THE EDGE OF THE GRASS BLUFF.
Observed: 2014-04-19T12:45:00Z
Source: OPUS - page5 1209.04



Close-up View

REF_FRAME:	EPOCH:	SOURCE:	UNITS:	SET PROFILE	DETAILS
NAD_83(2011)	2010.0000	NAVD88 (Computed using GEOID18)	m		
LAT: 40° 36' 45.78159" ± 0.005 m LON: -74° 3' 39.92633" ± 0.006 m ELL HT: -20.306 ± 0.023 m X: 1331507.398 ± 0.006 m Y: -4662274.018 ± 0.014 m Z: 4129856.450 ± 0.018 m ORTHO HT: 11.801 ± 0.052 m		UTM 18 SPC 3104(NY L) NORTHING: 4496190.068m 49533.655m EASTING: 579424.651m 294830.142m CONVERGENCE: 0.61120811° -0.03995830° POINT SCALE: 0.99967765 1.00000344 COMBINED FACTOR: 0.99968083 1.00000663			

CONTRIBUTED BY

[mike](#)
 [JOA Surveys, LLC](#)

Horizon View



The numerical values for this position solution have satisfied the quality control criteria of the National Geodetic Survey. The contributor has verified that the information submitted is accurate and complete.

OPUS Results for dockside TBM ML2022-01

FILE: 20220419_1814_30s.22o OP1650422676268

2005 NOTE: The IGS precise and IGS rapid orbits were not available
 2005 at processing time. The IGS ultra-rapid orbit was/will be used to
 2005 process the data.

NGS OPUS SOLUTION REPORT

=====

All computed coordinate accuracies are listed as peak-to-peak values.

For additional information: <https://www.ngs.noaa.gov/OPUS/about.jsp#accuracy>

USER: aunrein@thayermahan.com

DATE: April 20, 2022

RINEX FILE: 2022109s.22o

TIME: 02:47:07 UTC

SOFTWARE: page5 2008.25 master275.pl 16032 START: 2022/04/19 18:15:00

EPHEMERIS: igu22062.eph [ultra-rapid] STOP: 2022/04/19 22:36:00

NAV FILE: brdc1090.22n OBS USED: 9414 / 10897 : 86%

ANT NAME: HEMA45 NONE # FIXED AMB: 74 / 77 : 96%

ARP HEIGHT: 1.829 OVERALL RMS: 0.017(m)

REF FRAME: NAD_83(2011)(EPOCH:2010.0000) ITRF2014 (EPOCH:2022.2982)

X: 1330034.910(m) 0.002(m) 1330033.956(m) 0.002(m)

Y: -4660896.374(m) 0.009(m) -4660894.946(m) 0.009(m)

Z: 4131856.370(m) 0.003(m) 4131856.347(m) 0.003(m)

LAT: 40 38 11.48528 0.003(m) 40 38 11.51923 0.003(m)

E LON: 285 55 35.91970 0.003(m) 285 55 35.89734 0.003(m)

W LON: 74 04 24.08030 0.003(m) 74 04 24.10266 0.003(m)

EL HGT: -30.402(m) 0.008(m) -31.658(m) 0.008(m)

ORTHO HGT: 1.693(m) 0.052(m) [NAVD88 (Computed using GEOID18)]

UTM COORDINATES STATE PLANE COORDINATES

UTM (Zone 18) SPC (3104 NY L)

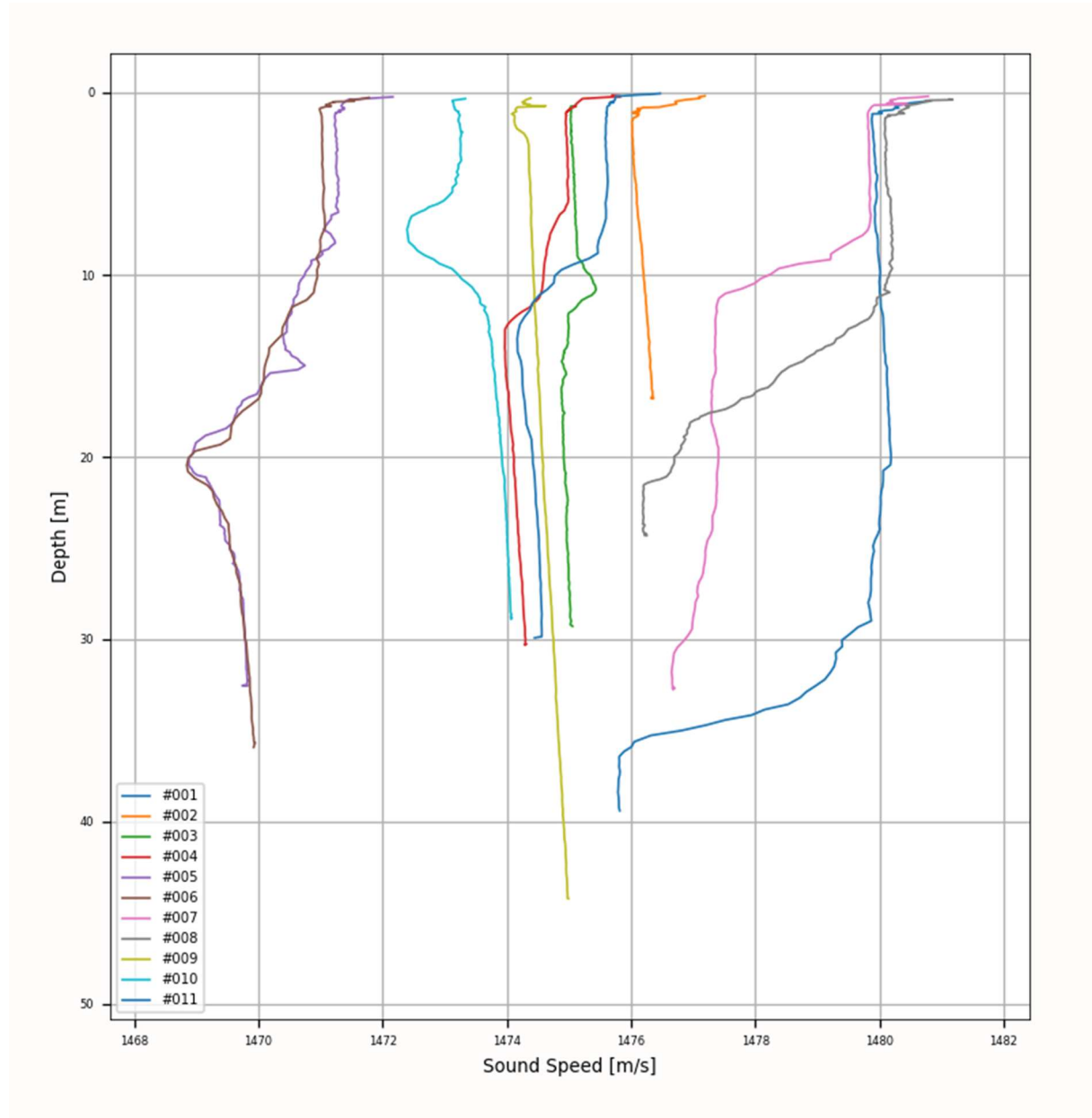
Northing (Y) [meters]	4498821.709	52178.099
Easting (X) [meters]	578359.281	293794.419
Convergence [degrees]	0.60351667	-0.04798056
Point Scale	0.99967558	1.00000181
Combined Factor	0.99968035	1.00000658

Collected Survey Sound Speed Profiles

Figure A- 15. Sound Speed Profiles.

Graph of all collected sound speed profiles.

(ThayerMahan, Inc.)



Sound Speed Calibration Certificates

Sound Speed Profiler 1 (A30520)



Certificate of Calibration

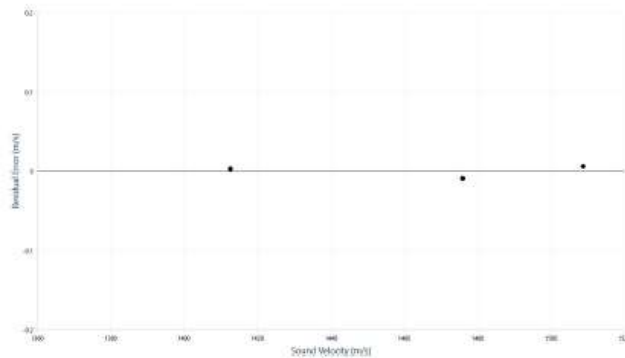
Serial Number: 210606	Calibration Range: 1412.596 to 1508.700 m/s
Calibration Date: 2022-04-02	Sensor Range: 1375-1625 m/s
Calibration Type: Sound Velocity (SVx2)	Standard: Hart Scientific 1560
RMSE: 0.007	

Calibration Data

Reference (m/s)	Sensor Output	Sensor Calculated (m/s)	Residual (m/s)
1508.7002	3406.13	1508.7064	0.0062
1475.8890	3481.90	1475.8799	-0.0092
1412.5962	3637.91	1412.5991	0.0029

Sensor Coefficients

A = 6.621954E-2
 B = -9.997988E-1



AML Oceanographic certifies that the asset described above has been calibrated or recalibrated with equipment referenced to traceable standards. If this instrument or sensor has been re-calibrated, please be sure to update your records. Please also ensure that you update the instrument's coefficient values in any post-processing software that you use, if necessary.



Certificate of Calibration

<p>Serial Number: 308221 Calibration Date: 2022-04-11 Calibration Type: Pressure (Px2) RMSE (%FS): 0.005</p>	<p>Calibration Range: -0.071 to 99.730 dBar Sensor Range: 100 dBar Standard: Paro Scientific 785</p>
---	---

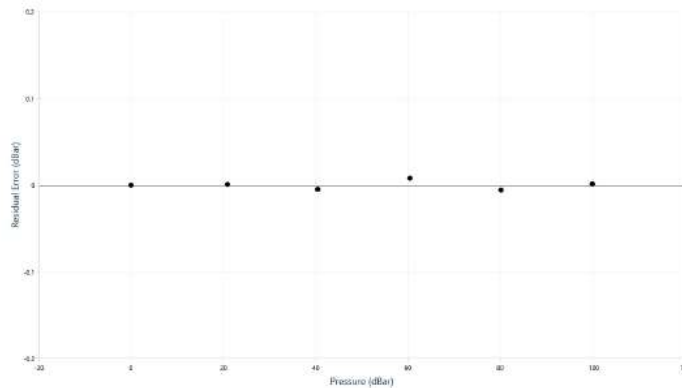
Calibration Data

Reference (dBar)	Sensor Output	Sensor Calculated (dBar)	Residual (% F.S.)
-0.0710	834060.15	-0.0709	0.0001
20.8391	2237197.00	20.8400	0.0009
40.4295	3553176.44	40.4247	-0.0048
60.4260	4898363.35	60.4340	0.0080
80.1834	6225238.82	80.1778	-0.0056
99.7304	7537801.00	99.7318	0.0015

Sensor Coefficients

A = -1.252296E+1
 E = 1.494160E-5
 I = -1.551664E-14
 M = 1.189882E-21

Equation: $P = A + E*x + I*x^2 + M*x^3$



AML Oceanographic certifies that the asset described above has been calibrated or recalibrated with equipment referenced to traceable standards. If this instrument or sensor has been re-calibrated, please be sure to update your records. Please also ensure that you update the instrument's coefficient values in any post-processing software that you use, if necessary.

Surface Sound Speed Sensor (80693)



CALIBRATION CERTIFICATE

This document certifies that the instrument detailed below has been calibrated according to Valeport Limited's Standard Procedures, using equipment with calibrations traceable to UKAS or National Standards.

Calibration Certificate Number:	70757
Instrument Type:	miniSVS
Instrument Serial Number:	80693
Calibrated By:	N. Paddon
Date:	10/03/2022
Signed:	

Full details of the results from the calibration procedure applied to each fitted sensor are available, on request, via email. This summary certificate should be kept with the instrument.



Valeport Limited
St. Peter's Quay, Totnes,
Devon TQ9 5EW UK

+44 (0) 1803 869292
sales@valeport.co.uk
www.valeport.co.uk

SVS Inc. 09 025 6703 97
Registered in England No. 1629466



Appendix B: Data Package Contents

The list below breaks down the contents of the data package deliverable. The included file types and the recommended support software is listed under Relevant Software.

Digital Deliverables Folder/File structure.

- **(Folder) MBES**
 - General file format: xxxx_yyyy_zzzz_##cm_” rev”#.
 - xxxx – Location (Either BIWF or LIS).
 - yyyy – MBES system (Norbit or R2Sonic).
 - zzzz – (optional) Area Description.
 - ##cm – Resolution (All bathymetry processed at 50cm).
 - rev# - (optional) Revision of processed file.
 - (.tiff) 50cm GeoTiff of bathymetric surface.
 - (.csar) Caris special archive file for storing bathymetric metadata.
 - (.csar0) Caris special archive file for storing bathymetric data.

- **(Folder) SAS**
 - (Folder) BIWF.
 - (Folder) North.
 - Contains all files associated with the Northern BIWF cable corridor.
 - (.tiff) 10cm GeoTiff mosaic.
 - (.tfw) File for georeferencing the GeoTiff raster image.
 - (.ovr) File containing the overlaid pyramid layers for the raster dataset.
 - (Folder) South.
 - Contains all files associated with the Southern BIWF cable corridor.
 - (.tiff) 10cm GeoTiff mosaic.
 - (.tfw) File for georeferencing the GeoTiff raster image.
 - (.ovr) File containing the overlaid pyramid layers for the raster dataset.
 - (Folder) Turbines.
 - Contains all files associated with the BIWF WTG’s.

- (.tiff) 10cm GeoTiff mosaic.
 - (.tfw) File for georeferencing the GeoTiff raster image.
 - (.ovr) File containing the overlaid pyramid layers for the raster dataset.
- (Folder) Wreck.
 - Contains all files associated with the wreck test site near the Northern BIWF cable corridor.
 - (.tiff) 10cm GeoTiff mosaic.
 - (.tfw) File for georeferencing the GeoTiff raster image.
 - (.ovr) File containing the overlaid pyramid layers for the raster dataset.
- (Folder) LIS.
 - (Folder) East – West.
 - Contains all files associated with the simulated targets while surveying along the parallels.
 - (.tiff) 10cm GeoTiff mosaic.
 - (.tfw) File for georeferencing the GeoTiff raster image.
 - (.ovr) File containing the overlaid pyramid layers for the raster dataset.
 - (Folder) Full Coverage.
 - Contains all files associated with the simulated target site.
 - (.tiff) 10cm GeoTiff mosaic.
 - (.tfw) File for georeferencing the GeoTiff raster image.
 - (.ovr) File containing the overlaid pyramid layers for the raster dataset.
- **(Folder) Target Tif Imagery**
 - (Folder) Targets.
 - (Folder) Port.
 - Contains all individual tile imagery files associated with the Port sonar.
 - (Folders) Sub-folders A thru E.
 - (.tiff) All GeoTiffs relevant to each target.
 - (.txt) Listing of relevant GeoTiffs.
 - (Folder) Stbd.
 - Contains all individual tile imagery files associated with the Port sonar.

- (Folders) Sub-folders A thru E.
 - (.tiff) All GeoTiffs relevant to each target.
 - (.txt) Listing of relevant GeoTiffs.
 - (.xlsx) **NOWRDC ATR Line Report.**
 - Spreadsheet of survey lines, target files, and corresponding simulated target imagery.
- **(.xlsx) 2022-0402 OperationsLog**
 - Operations log of survey lines and daily system checks.

Appendix C: ATR Algorithm

ATR Prior Studies

Original Study

The first study conducted on the performance of ATR on seabed entities on our SAS imagery was conducted over eight different classes with varying number of instances over 5,270 images as detailed in Table C- 1 below. It should be noted that this dataset has since increased in instances across all classes since this experiment was first conducted.

Table C- 1. AI ATR Study Results.

Number of total instances and percent of total instances in ATR study 1.

(ThayerMahan, Inc.)

	# Total Instances	% Total Instances	# in Train	# in Val	# in Test
Block	75	0.83%	60	12	3
Line	408	4.53%	327	73	48
Man-Made	1234	13.70%	860	246	128
Natural	836	9.28%	593	172	119
Pot	2211	24.54%	1584	405	222
Rock	2956	32.82%	2026	593	337
Unknown	1270	14.10%	1660	423	242
Wreck	18	0.20%	11	3	4

These samples were equally distributed into train, validation, and testing sets of 70/20/10 splits, and preprocessed via our patented tiling method. We trained our algorithm utilizing pre-trained YOLOv5l (“large”) weights on the COCO dataset and conducted transfer learning on our unique dataset.

The results of this experiment are listed below in Table C- 2, and the weighted scores of our algorithm are detailed below.

Table C- 2. ATR Precision Scores.

Accuracy and precision scores. Weighted values in the bottom table.

(ThayerMahan, Inc.)

	Accuracy	Precision	Recall	F1-Score
Block	100%	0.75	1	0.86
Line	16%	0.89	0.16	0.28
Man-Made	37%	0.77	0.37	0.5
Natural	7%	0.35	0.07	0.11
Pot	68%	0.84	0.69	0.76
Rock	41%	0.77	0.42	0.54
Unknown	38%	0.61	0.39	0.47
Wreck	33%	1	0.33	0.5

Weighted Precision	0.71
Weighted Recall	0.41
Weighted F1-Score	0.51

Given the results of the weighted scores, it’s apparent that our algorithm prioritizes generating bounding box detections (high precision), a deprioritizes generating accurate bounding boxes (low recall). This may be a preferable outcome since we want to detect all anomalies within the images at the sake of correctness of those inferred class labels.

As a note of improvement, we identified that there is a drastic class imbalance that would need to be assuaged in order to improve our algorithms performance on the under-represented classes.

Unequal Distribution of Class Representation Analysis

During investigations into model performance, we conducted an ablation study to determine if the drastic class instance imbalance shown in our database resulted in reduced performance. The break-down of our original classes are shown above in Table C- 2. It is important to distinguish that an image may have more than one instance of a class, so conducting this study over a classes number of instances over all images as opposed to the number of images that a class is a part of is necessary. As shown in the table, our most represented classes, such as Pots and Rocks far outweighed the class representation of classes such as Blocks, Lines, and Wrecks.

In our ablation study, we created six datasets of three different categories, consisting of unique instances within our dataset. Each dataset consists of 2,400 samples with a 70/20/10 train, validation, and testing splits and preprocessed on our patented tiling method. The first two datasets consisted of a balanced representation over all classes, where each class represented 400 samples in the dataset. The second two datasets consisted of a control, consisting of class representations equal to the percentage of total instances in the original dataset (from Table C1 column “% Total Instances” above). The last two datasets comprised of a random distribution of instances across all classes. The break-down of representation can be found below in Table C- 3.

Table C- 3. Class Distribution.

Random distribution of instances across all classes and representation.

(ThayerMahan, Inc.)

Class	Bal A & B	Cont A & B	Random A	Random B
Line	400 (16.6%)	107 (4.45%)	213 (8.9%)	203 (8.95%)
Man-Made	400 (16.6%)	294 (12.27%)	726 (30.25%)	637 (26.54%)
Natural	400 (16.6%)	211 (8.78%)	311 (12.95%)	127 (5.29%)
Pot	400 (16.6%)	528 (21.98%)	596 (24.83%)	583 (24.29%)
Rock	400 (16.6%)	705 (29.38%)	106 (4.42%)	695 (28.95%)
Unknown	400 (16.6%)	555 (23.11%)	448 (18.66%)	155 (6.45%)

The results of the ablation study are shown below in Table C- 4. What stands out the most from our study is the consistent high performance our ATR algorithm has on the Pot class. This may be due to the Pot class having very distinct shapes of relatively low variability, strong edges, and a non-reliance on shadows for classification. As for the performance of the Line class, we hypothesize that due to the shape of the bounding box annotation containing great amounts of background around the object (problematic in instances where the Lines are not completely horizontal or vertical. With a pixel-perfect annotation representation (such as with Instance Segmentation methods), we postulate that performance on this class specifically, and all classes overall, would improve dramatically. In terms of the performance of the Rock, Man-Made, and Natural classes, it is evident that there is great ambiguity within each class, and across

each of the classes. For instance, in some areas with high rock density, those instances may be annotated as Natural as opposed to each unique Rock being annotated individually. We conclude that not only is there an imbalance of class representations, but there also exists improvements over the class structure we adhere to for classification.

Table C- 4. Ablation Study.

Ablation study results across classes.

(ThayerMahan, Inc.)

	Balanced A	Balanced B	Control A	Control B	Random A	Random B	All Sets
Line	3.3	4.8	0.0	0.1	2.4	0.9	1.9
Man-Made	16.7	2.5	2.3	6.5	10.6	20.7	9.8
Natural	5.7	3.6	0.6	2.8	10.2	0.2	3.8
Pot	37.1	26.2	26.0	45.2	36.5	25.2	32.7
Rock	1.6	1.8	1.6	2.0	0.1	0.8	1.3
Unknown	3.5	7.4	5.4	7.7	6.3	1.9	5.3
All Classes	11.3	7.7	6.0	10.7	11.0	8.3	

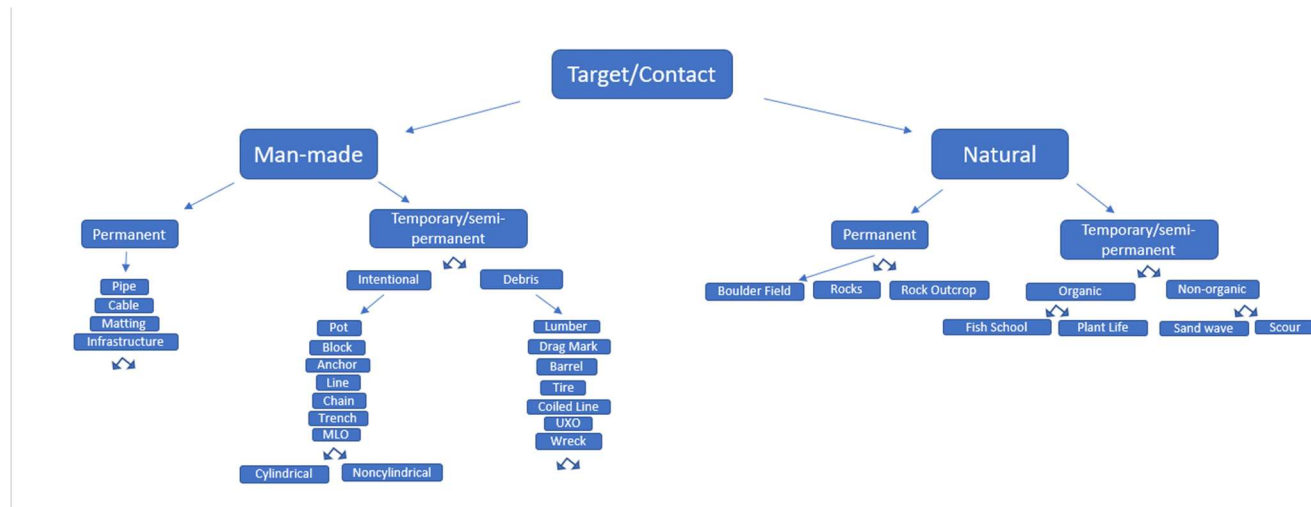
Creating a Hierarchical Labeling Approach

The previous ablation study highlighted the need for consistent annotation labeling and the creation of more fine-grained and unique class labels to reduce ambiguity amongst classes, detailed in Figure C-1 below.

Figure C- 1. Class Labels.

Annotation labeling and unique class labels.

(ThayerMahan, Inc.)



Comparing this graph class structure, which consists of 27 “leaf” classes, to the prior class structure, which consisted of only 6 classes, there exists a trade-off between keeping the class structure generic and minimal to increase the number of instances per-class and creating a more fine-grained class structure which represents each unique entity as its own class, at the sake of reduced instances per-class. As such, instead of treated each class distinction equally across the entire dataset, we propose our hierarchical labeling schema as the gold standard for conducting ATR for seabed entities.

The benefit of creating this hierarchical structure is such that if our ATR algorithm misclassifies an entity, for instance, mistakes an upright Barrel for a Tire, we can reduce the effects of a misclassification, since both the Barrel and Tire classes are from the same parent class Debris. In this way, we can train our ATR algorithm on unique and non-ambiguous classes while acknowledging that the model may fail to correctly differentiate leaf classes but may correctly determine which hierarchical parent an entity belongs to.

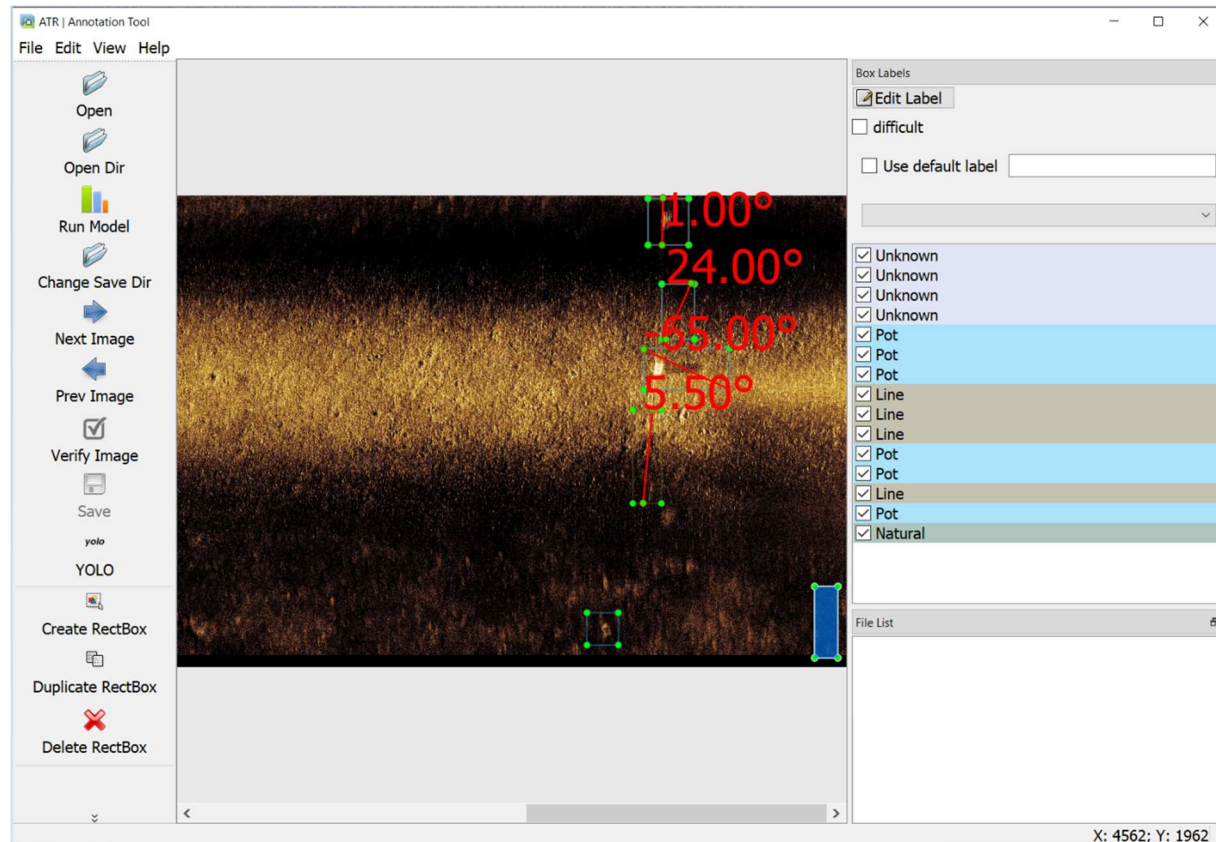
Appendix D: “sGUId” ATR Annotation Tool

ThayerMahan Inc. currently utilizes the open-source labeling platform from Heartex Laboratories to facilitate the curation of annotations for our SAS imagery. A screenshot of the labeling platform is shown below in Figure D-1, with a few modifications to its design for our curation process. The goal in utilizing an annotation tool is to drastically reduce the time it takes for an operator to analyze and annotate the SAS imagery following the data exfiltration process.

Figure D- 1. Labelling Annotation Tool.

Screenshot of the Labeling platform from Heartex Laboratories used in curation of SAS imagery annotations.

(ThayerMahan, Inc.)



Augmenting the original labeling platform, we’ve included the ability to conduct ATR inference over the loaded images after they’re loaded into the interface. Once completed, the images will have bounding box annotations associated with them, consisting of the output we receive from our ATR model, YOLOv5. Preprocessing the data in this way has already reduced the amount of time required to complete the

review and analysis process of our SAS imagery by about 30%. We are continuing to improve proficiency throughout internal testing and iteration.

Additionally, we've developed a separate algorithm to take Line detections, and break them up into separate line segments, such that we can output the angle at which the line segments lie, relative to true north (being the top-center of the captured image).

At ThayerMahan Inc., we face a great challenge we refer to as the "100:1" problem – how do you enable a single operator to manage over 100 unique sensor modalities in real-time. We adhere to this mindset in our "sGUId" product (est. version alpha by end of Q4 2022) by preprocessing the data beforehand, so an operator can receive contact reporting on a much faster scale than if they had to do so manually.